

Hypernuclear physics with pions

C. B. Dover

Brookhaven National Laboratory, Upton, New York 11973

L. Ludeking and G. E. Walker

Physics Department, Indiana University, Bloomington, Indiana 47405

(Received 23 May 1980)

We investigate the possibility of producing hypernuclei with energetic pion beams via the (π^+, K^+) reaction. Due to the high momentum transfer involved ($q \approx 300$ MeV/c), even in the forward direction, the (π^+, K^+) reaction preferentially populates high spin natural parity configurations obtained by coupling a Λ particle to a neutron hole. We present differential cross section calculations utilizing the plane wave approximation (PWA), the distorted wave impulse approximation (DWIA) using fully distorted waves, and the eikonal approximation (EIK) to approximate distortion effects. The DWIA and EIK results are in agreement, and lead to cross sections typically a factor of 5–10 lower than the PWA results, due to absorptive effects. Cross sections of 5–20 μ b/sr at 0° are obtained in the DWIA for high spin natural parity “stretched configurations,” for example $(\Lambda d_{3/2,5/2} \otimes n f_{7/2}^{-1})^{5-}$ or $(\Lambda f_{5/2,7/2} \otimes n f_{7/2}^{-1})^{6+}$ in ${}^{48}\text{Ca}$, for pion lab momentum p_π in the range 1.02–1.1 GeV/c, where the elementary cross section for $K^+ n \rightarrow \pi^+ \Lambda$ has its peak values. The cross sections for the population of the natural parity ground-state levels $(\Lambda S_{1/2} \otimes n l_{l+1/2}^{-1})_{J=l}$ with closed shell targets remain above 2 μ b/sr at 0° for systems lighter than $A \approx 50$. The cross sections drop rapidly below $p_\pi = 1.02$ GeV/c, due to threshold effects. Results are presented for the calculated quasielastic (quasifree) continuum background for the (π^+, K^+) reaction as a function of θ_{lab} and hypernuclear excitation energy. Because of the higher momentum transfer the quasielastic background is broader and significantly less in magnitude than that obtained in the (K^-, π^-) reaction at 0° . Thus it should be possible to measure cross sections of a few μ b/sr associated with particle-hole states using existing pion beams in the 1–1.5 GeV/c momentum range, for instance at the Brookhaven AGS. The class of hypernuclear states populated at 0° in a (π^+, K^+) reaction is complementary to those seen in the “crossed” (K^-, π^-) reaction at 0° , the latter being sensitive only to low spin states. Thus the (π^+, K^+) reaction offers unique possibilities for extending our knowledge of hypernuclear structure.

[NUCLEAR STRUCTURE Excitation of high spin states in (π, K) reaction.
DWIA and PWA estimates of cross sections.]

I. INTRODUCTION

The earliest studies of hypernuclear structure involved emulsion techniques.¹ This method, with minor exceptions, is restricted to the ground states of light hypernuclei ($A < 16$), since one must see the decay $\Lambda \rightarrow p \pi^-$ into charged products, and this mode is greatly inhibited in heavy systems due to the effects of the Pauli principle on the recoiling proton.² More recently,³ pioneering experiments were done at CERN using the (K^-, π^-) and (K^-, π^+) reactions to form various excited Λ and Σ hypernuclear states. The elementary $K^- n \rightarrow \pi^- \Lambda$, $\pi^- \Sigma^0$, and $K^- p \rightarrow \pi^+ \Sigma^-$ processes are exothermic, and there exists a “magic momentum” for which the momentum transfer at $\theta_{\text{lab}} = 0^\circ$ is zero.⁴ The resulting slow Λ or Σ has a sizable probability for sticking in the nucleus, in particular to form recoilless substitutional 0^+ states³ where the hyperon replaces a neutron in the same shell model orbital. Cross sections of a few tenths of a millibarn (as

large as 1 mb/sr) are typical for the excitation of 0^+ states via the (K^-, π^-) reaction in light hypernuclei. For $J \neq 0$ states, the (K^-, π^-) cross sections peak at finite angle, with peak cross sections considerably reduced relative to those for 0^+ states. For instance, measurements of (K^-, π^-) angular distributions at Brookhaven⁵ have yielded evidence for the excitation of 2^+ states in ${}^{12}\text{C}$ at a peak level of 0.1 mb/sr. It is clear that the (K^-, π^-) reaction at forward angles emphasizes the spectroscopy of low spin hypernuclear states, at least for spin zero targets.

Existing kaon beams⁶ have an intensity of a few times 10^4 kaons/burst. This low intensity means that only coarse energy resolution ($\Delta E \approx 2$ –6 MeV) experiments are feasible at present. Due to the much higher beam intensities available with other projectiles such as pions, protons, and heavy ions, alternative methods of producing hypernuclei have been suggested. These include

- (a) $(N, Z) + p \rightarrow {}_{\Lambda}(N-1, Z) + n + K^+$,
 (b) $p + (N, Z) \rightarrow {}_{\Lambda}(N, Z-1) + p' + K^+$,
 (c) $p + (N, Z) \rightarrow {}_{\Lambda}(N, Z) + K^+$,
 (d) $\pi^+ + (N, Z) \rightarrow {}_{\Lambda}(N-1, Z) + K^+$,
 (e) $\gamma + (N, Z) \rightarrow {}_{\Lambda}(N, Z-1) + K^+$,
 (f) $e + (N, Z) \rightarrow {}_{\Lambda}(N, Z-1) + e' + K^+$.

Reaction (a) has been studied by bombarding a hydrogen target with high energy heavy ions.⁷ The ground state lifetime of ${}_{\Lambda}^{16}\text{O}$ was measured in this way, but this type of experiment is not appropriate to a detailed study of hypernuclear spectroscopy. Reactions (b) and (c) are similar, except that the presence of the continuum proton in (b) reduces the momentum transfer somewhat, and hence the Λ may more readily "stick" to the nucleus than in reaction (c). Theoretical estimates⁸ exist, but preliminary experimental results from Saturne⁹ have not indicated any measurable cross section for the formation of *discrete* hypernuclear states in (b).

All of the reactions listed in Eq. (1.1) are endo-ergic, unlike the (K^-, π^+) process, and there is no magic momentum of the projectile at which the Λ is produced with zero momentum in the nucleus, at least for the two-body processes (c), (d), and (e). Therefore, even at forward angles, one would not expect to populate *low spin* hypernuclear states in these reactions. The lab kinetic energies corresponding to the thresholds for inducing these reactions on a very heavy target at rest are given by

$$\begin{aligned} T_p &\approx 530 \text{ MeV for } (\pi^+, K^+), \\ T_p &\approx 670 \text{ MeV for } (p, K^+), \\ E_\gamma &\approx 670 \text{ MeV for } (\gamma, K^+), \end{aligned} \quad (1.2)$$

neglecting binding energy corrections. These thresholds are effectively reduced¹⁰ somewhat if one considers Fermi motion in the nucleus ("sub-threshold production"). The (π^+, K^+) reaction is near the upper end of the range of energy of the pion factories at LAMPF, SIN, and TRIUMF, although such experiments would be feasible using the separated beams available at a higher energy accelerator, for instance the Brookhaven AGS. The production of hypernuclei via the (γ, K^+) reaction is similar kinematically to the (π^+, K^+) reaction, although the spin of the photon enables one to excite unnatural as well as natural parity states.¹¹ The $(e, e'K^+)$ process corresponds to (γ, K^+) with a virtual photon and may be considered with the

advent of higher energy electron accelerators.¹¹

In the present article, we focus on the possibility of studying hypernuclear physics with pion beams, via the (π^+, K^+) reaction. Since the momentum transfer q remains larger than the Fermi momentum K_F in the entire momentum region where the two body process $\pi^+n \rightarrow K^+\Lambda$ is large, the cross sections for forming the low spin states seen in (K^-, π^-) will be very small. However, we demonstrate that the *highest spin* states formed by coupling a Λ and a neutron hole in a "stretched" configuration are excited with measurable cross sections at 0° of at least $10 \mu\text{b}/\text{sr}$. The states seen in the (π^+, K^+) reaction are complementary to the "recoiles" 0^+ peaks [e.g. $({}_{\Lambda}p_{3/2} \otimes {}_n p_{3/2}^{-1})_{0^+}$ in ${}_{\Lambda}^{12}\text{C}$] which are strongly picked out by the (K^-, π^-) reaction. Thus a new domain of hypernuclear physics can be studied via this process.

The paper is organized as follows: In Sec. II, we review the properties of the elementary $\pi N \rightarrow K\Lambda$ amplitude. We focus on the properties of interest for hypernuclear physics; that is, the dependence of the 0° differential cross section and momentum transfer q on the incident pion momentum. In Sec. III, we discuss our calculational procedures and the DWIA, the basic formalism for discussing the (π, K) process. The application of the full DWIA formalism is briefly summarized, along with the choice of optical potentials for the π^+ and K^+ channels. Also included is a discussion of the nuclear quasielastic response. The results of calculations of the (π^+, K^+) cross sections in the plane wave impulse approximation (PWA) are presented in Sec. IV with emphasis on the strongly excited high spin states. The PWA calculations produce the correct angular shapes, and enable us to understand the full DWIA results in a simpler way. In Sec. V, we display the systematics of the (π^+, K^+) cross sections as a function of pion momentum, target mass, and spin of the residual hypernucleus, using the eikonal approximation for the distorted waves. The sensitivity of the results to the choice of potential (oscillator or Woods-Saxon) for the n and Λ bound states is discussed. For some particular cases, we show that the eikonal results agree well with the full DWIA calculations. Also in Sec. V, the quasielastic (QE) contribution to the (π^+, K^+) cross section is examined. Because of the large value of q , the QE spectrum is very flat in energy, unlike the situation for the low q (K^-, π^+) reaction. We show that narrow peaks due to the excitation of particular high spin Λ particle- n hole states should be readily resolvable from the QE background. Finally, we explore the general outlook for investigations of hypernuclear structure via the (π^+, K^+) reaction.

II. KINEMATICAL CONSIDERATIONS AND THE ELEMENTARY (π^+, K^+) AMPLITUDES

The associated production reaction $\pi N \rightarrow \Lambda K$ has been extensively studied experimentally. The most recent papers, which contain references to earlier work, are those of the Rutherford group.¹²⁻¹⁵ In Refs. 12-14, the data on the process $\pi^- p \rightarrow K^0 \Lambda$ from threshold to 2375 MeV/c are subjected to a partial wave analysis. Data on the $\pi^- p \rightarrow K^0 \Sigma^0$ reaction are also available.¹⁵

For a hypernuclear physics experiment, using a charged particle magnetic spectrometer to detect the final state kaon, the relevant process is $\pi^+ n \rightarrow K^+ \Lambda$ or $K^+ \Sigma^0$. Charge independence gives the following relation between the amplitudes f :

$$f_{\pi^+ n \rightarrow K^+ \Lambda} = -f_{\pi^- p \rightarrow K^0 \Lambda}, \quad (2.1)$$

$$f_{\pi^+ n \rightarrow K^+ \Sigma^0} = f_{\pi^- p \rightarrow K^0 \Sigma^0},$$

so the (π^+, K^+) cross sections needed are identical to the measured (π^-, K^0) values. In the two body systems, the lab threshold momenta p_π^T are the following:

$$p_\pi^T = \begin{cases} 0.89 \text{ GeV/c for } \pi^+ n \rightarrow K^+ \Lambda, \\ 1.02 \text{ GeV/c for } \pi^+ n \rightarrow K^+ \Sigma^0, \end{cases} \quad (2.2)$$

corresponding to pion lab kinetic energies of $T_\pi = 760$ and 890 MeV for $K^+ \Lambda$ and $K^+ \Sigma^0$, respectively. On a heavy nuclear target, the thresholds for associated production are lower: we find $T_\pi = 530$ and 607 MeV for Λ or Σ^0 production.

The tabulated results of Refs. 12-14 refer to differential cross sections $(d\sigma/d\Omega)_{\text{c.m.}}$ in the two-body center of mass system. For our later calculations of hypernucleus production, we find it more convenient to work in the many-body lab system. We first transform the $\theta = 0^\circ$ cross section for $\pi^+ n \rightarrow K^+ \Lambda$ from the two body c.m. to the two body lab frame via the relation

$$\frac{(d\sigma/d\Omega)_{L,0^\circ}^{\pi^+ n \rightarrow K^+ \Lambda}}{(d\sigma/d\Omega)_{\text{c.m.},0^\circ}^{\pi^+ n \rightarrow K^+ \Lambda}} = \left(\frac{k_{K^+ L}}{k_{K^+}} \right)^2, \quad (2.3)$$

where $k_{K^+ L}$ and k_{K^+} are the lab and c.m. momenta of the K^+ , respectively. To compute the ratio in Eq. (2.3), we start with the pion lab momentum $k_{\pi L}$ and obtain the pion c.m. momentum k_π from

$$k_\pi = k_{\pi L} (1 + m_\pi^2/m_N^2 + 2\epsilon_{\pi L}/m_N)^{-1/2}, \quad (2.4)$$

where $\epsilon_{\pi L} = (m_\pi^2 + k_{\pi L}^2)^{1/2}$. In terms of k_π , we now obtain $k_{K^+ L}$ at $\theta = 0^\circ$ and k_{K^+} from the relations

$$\begin{aligned} k_{K^+ L} &= (\epsilon_{K^+ L}^2 - m_{K^+}^2)^{1/2}, \\ \epsilon_{K^+ L} &= [\beta_1(\epsilon_{\pi L} + m_N) + k_{\pi L}(\beta_1^2 - m_{K^+}^2 \beta_2)^{1/2}]/\beta_2, \\ \beta_2 &\equiv m_N \epsilon_{\pi L} + (m_N^2 + m_{K^+}^2 + m_\pi^2 - m_\Lambda^2)/2, \\ \beta_1 &\equiv m_\pi^2 + m_N^2 + 2\epsilon_{\pi L} m_N \end{aligned} \quad (2.5)$$

and

$$k_{K^+} = \left(\frac{(\beta_3 - \beta_4)^2 - m_{K^+}^2 m_\Lambda^2}{m_N^2 - m_\pi^2 + 2\beta_3} \right)^{1/2}, \quad (2.6)$$

$$\beta_3 \equiv \epsilon_\pi (\epsilon_\pi + \epsilon_N),$$

$$\beta_4 \equiv \frac{1}{2}(m_\pi^2 + m_{K^+}^2 + m_\Lambda^2 - m_N^2),$$

where $\epsilon_\pi = (m_\pi^2 + k_\pi^2)^{1/2}$ and $\epsilon_N = (m_N^2 + k_\pi^2)^{1/2}$.

In relating the two-body cross section $(d\sigma/d\Omega)_{L,0^\circ}^{\pi^+ n \rightarrow K^+ \Lambda}$ to the $\theta_L = 0^\circ$ formation cross section on a nuclear target, it is necessary to include a further kinematical factor α arising from the transformation from the two body to many body lab systems (i.e., the recoiling Λ has a different momentum in the two cases). This point is discussed in detail in Goldberger and Watson.¹⁶ As we show in Sec. III, the factor α enters as follows:

$$\left(\frac{d\sigma}{d\Omega} \right)_{L,0^\circ}^{\pi^+ n \rightarrow K^+ \Lambda Z^*(J^\pi)} = \alpha \left(\frac{d\sigma}{d\Omega} \right)_{L,0^\circ}^{\pi^+ n \rightarrow K^+ \Lambda} N_{\text{eff}}^J, \quad (2.7)$$

where N_{eff}^J is the effective number of neutrons for a transition to a final state J^π , and α is given by

$$\alpha = 1 - q/v_{K^+ L} \epsilon_{\Lambda L}. \quad (2.8)$$

In Eq. (2.8), $q = k_{\pi L} - k_{K^+ L}$ is the 0° two-body momentum transfer in the lab, $v_{K^+ L} = k_{K^+ L}/\epsilon_{K^+ L}$, and $\epsilon_{\Lambda L} = (m_\Lambda^2 + q^2)^{1/2}$. Note that for the (K^-, π^-) reaction, where q is small, we have $\alpha \approx 1$ and hence Eq. (2.7) reduces to a well-known result.¹⁷ For the $\pi^+ n \rightarrow K^+ \Lambda$ reaction, on the other hand, q is of the order of 275-325 MeV/c and α differs appreciably from unity, always tending to *reduce* the nuclear cross section.

In Fig. 1, we display the dependence of α and the cross section ratio $(d\sigma/d\Omega)_{L,0^\circ}/(d\sigma/d\Omega)_{\text{c.m.}}$ on the incident pion momentum. The product $\alpha(d\sigma/d\Omega)_{L,0^\circ}^{\pi^+ n \rightarrow K^+ \Lambda}$ which enters in Eq. (2.7) is shown in Fig. 2. Note that this product displays a rather sharp peak near $p_{\pi L} \approx 1.04$ GeV/c, although Fermi averaging would smooth this out somewhat. It is typical of particular two body processes that the peak cross section is achieved not far above threshold (here 0.89 GeV/c). At higher momenta, many other channels open up ($\pi^+ n \rightarrow K^+ Y^*$, $K^* \Lambda$, etc.) and the importance of the channel of interest diminishes. Hence, *a priori*, one might guess that an optimum momentum for (π^+, K^+) production of Λ hypernuclei would be around $p_{\pi L} \approx 1.04$ GeV/c. However, one must also consider the dependence of N_{eff}^J on q . In Fig. 3, we show how $q(0^\circ)$ depends on $p_{\pi L}$ for the processes $\pi^+ n \rightarrow K^+ \Lambda$, $K^+ \Sigma^0$. We also show the more familiar cases $K^- n \rightarrow \pi^- \Lambda$, $\pi^- \Sigma^0$ for comparison. This figure displays the striking difference between the exoer-

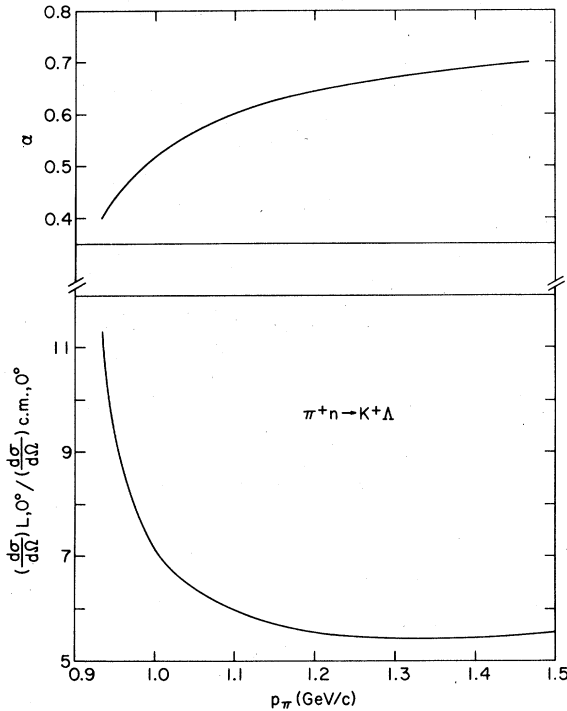


FIG. 1. Kinematical factors which enter the computation of the (π^+, K^+) cross section on a nuclear target. We show the quantity α of Eq. (2.8) in the top part of the figure as a function of the lab pion momentum p_π . In the lower half, we display the ratio of $\theta = 0^\circ$ differential cross sections in the two body lab and c.m. systems for the $\pi^+ n \rightarrow K^+ \Lambda$ process, as per Eq. (2.3).

gic (\bar{K}, π) and the endoergic (π, K) reaction. For the latter case, the momentum transfer q remains larger than the Fermi momentum K_F in the entire region of interest of p_π . Thus it is clear that the low spin states picked out by the (\bar{K}, π) process at 0° are very poorly matched in the (π, K) reactions, which emphasizes high spin states. The information obtained at forward angles on hypernuclear structure is quite complementary for the two processes. We explore this complementarity in more detail in the next section. Of course at angles of $\approx 20^\circ$ in the (\bar{K}, π) reaction one may excite states of spin large enough to be seen also in the (π, K) reaction. The idea of using two different processes to study the same hypernuclear state, for a few cases, is attractive because it may allow one to determine unsuspected reaction mechanism complications.

III. THEORETICAL PROCEDURES AND RELEVANT FORMULAS

A. General formalism for fully distorted waves

The basic formalism we adopt for studying the (π^+, K^+) reaction is the distorted wave impulse ap-

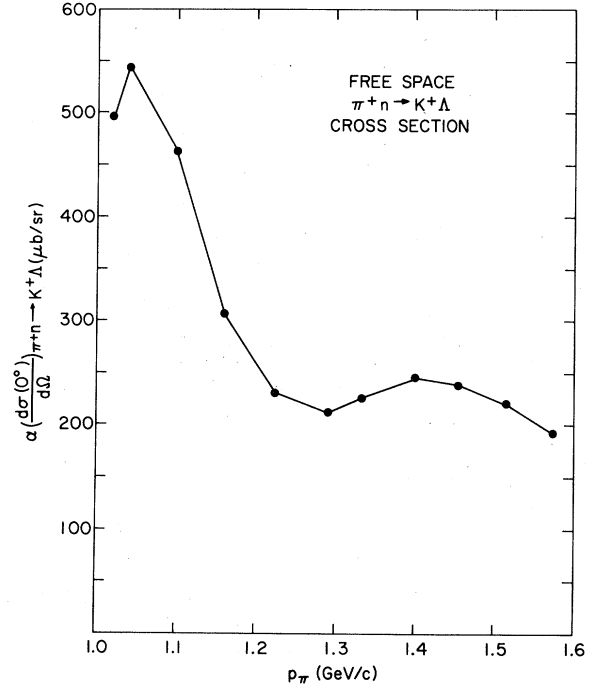


FIG. 2. Momentum dependence of the free space lab differential cross section at 0° for the $\pi^+ n \rightarrow K^+ \Lambda$ reaction. We include the kinematical factor α of Eqs. (2.7) and (2.8).

proximation. The procedure adopted follows closely that already applied to pion and kaon inelastic scattering if fully distorted waves are adopted.^{18,19} In the case of eikonal approximations for the distorted waves the procedure is similar to that adopted in Ref. 17 for the (K^-, π^-) reaction.

The basic input required for the DWIA calculations include: (a) distorted waves $\chi^{(\mp)}$ for the entrance (π^+) and exit (K^+) channels, (b) a two body transition amplitude $f_E(\vec{k}, \vec{k}')$ for the elementary $\pi^+ n \rightarrow K^+ \Lambda$ process appropriate for introducing into the many-baryon system, and (c) initial nuclear target and final hypernuclear many-particle wave functions.

First we consider the general formalism where one uses distorted waves generated from an optical potential.^{18,19} We have made a partial wave decomposition of the momentum space distorted waves. After a Fourier transform, we then expand the configuration space partial waves $\chi_E^{\pm}(p_i, r_k)$ in terms of Bessel functions $j_l(k_n r_k)$ with weights $a_{nl}(p_i)$, where the momenta $\{k_n\}$ have been chosen so that $j_0(k_n r_k)$ vanishes at $r_k = 12$ fm. In momentum space, we then obtain

$$\chi_E^{\pm}(p_i, k) = \frac{\pi}{2k^2} \sum_n a_{nl}(p_i) \delta(k_n - k). \quad (3.1)$$

In Refs. 18 and 19, a separable form for the ele-

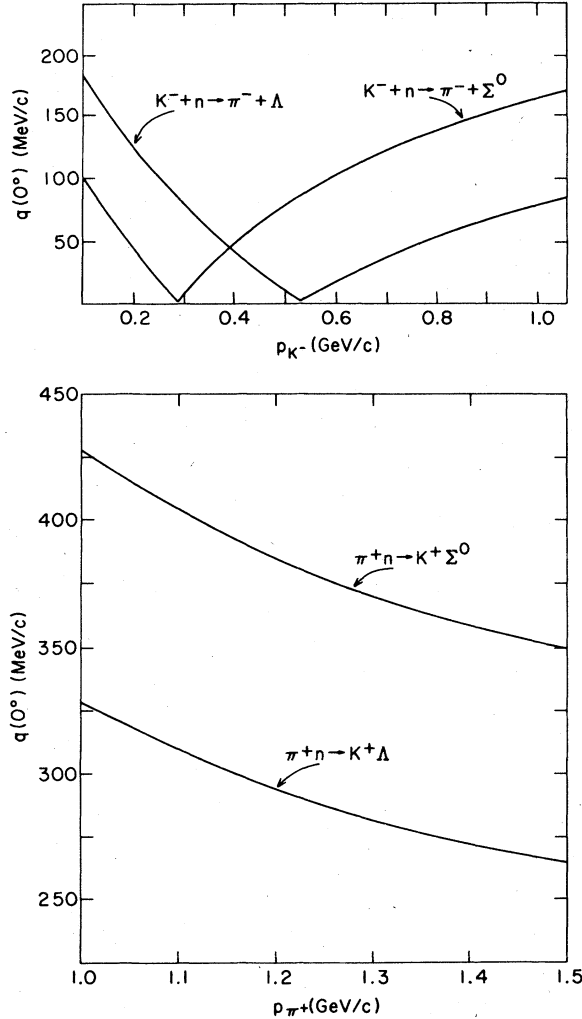


FIG. 3. The lab momentum transfer q at $\theta_L = 0^\circ$ as a function of incident lab momentum for the processes $K^- + n \rightarrow \pi^- + \Lambda$, $\pi^- + \Sigma^0$ and $\pi^+ + n \rightarrow K^+ + \Lambda$, $K^+ + \Sigma^0$ on a heavy target nucleus. Many body kinematics is used to calculate q , neglecting binding energy changes and assuming the target to be at rest in the lab.

mentary transition operator $f_E(\vec{k}, \vec{k}')$ was assumed, and the full partial wave expansion was used. Off-shell form factors and spin flip amplitudes were also included. For kaon inelastic scattering,¹⁹ it was found that off-shell effects had very little influence on cross sections, particularly for higher kaon momenta (800 MeV/c or so). An application of the same formalism to (K^-, π^-) reactions²⁰ revealed that the spin-flip cross sections to unnatural parity hypernuclear states were very small. We expect a similar situation to prevail for the (π^+, K^+) reaction, so for these first calculations we have neglected off-shell effects and spin-flip contributions to the $\pi^+ n \rightarrow K^+ \Lambda$ amplitudes. Instead of the full partial wave series, we have

used an effective s -wave parametrization for this amplitude:

$$\text{Im} f_{\pi^+ n \rightarrow K^+ \Lambda}^{1ab} = \left[\alpha \left(\frac{d\sigma}{d\Omega} \right)_{L, 0^\circ}^{\pi^+ n \rightarrow K^+ \Lambda} \right]^{1/2}. \quad (3.2)$$

We assume $\text{Re} f = 0$ and include the kinematical factor α of Eq. (2.8) in the definition of $\text{Im} f$. The laboratory cross section $(d\sigma/d\Omega)_{L, 0^\circ}$ is obtained via Eq. (2.3) from the tabulated c.m. cross sections. The assumption (3.2) is equivalent to using a zero range approximation to f in coordinate space, since then we get only an s -wave amplitude, i.e., we neglect the angular (momentum transfer) dependence of the elementary process. This approximation has also been made in all calculations of the (K^-, π^-) reaction to date,^{17,21} except for that of Ref. 20, which uses the full partial amplitudes for $K^- n \rightarrow \pi^- \Lambda$. Note that as an approximation to the two-body amplitude, an s -wave assumption is very poor, since many N^* resonances are present for $\pi^+ n \rightarrow K^+ \Lambda$ or Y^* resonances for $K^- n \rightarrow \pi^- \Lambda$, even close to threshold. Higher partial waves are an essential part of the two body problem. However, the angular shape of the (π^+, K^+) or (K^-, π^-) cross sections on a nuclear target is primarily determined by the size of the nucleus and the question of how the total two body cross section is distributed among the various partial waves is less important. In Ref. 20, calculations employing quite different partial wave decompositions (but the same value of $(d\sigma/d\Omega)_{c.m.}^{K^- n \rightarrow \pi^- \Lambda}$) gave very similar cross sections for $^{12}\text{C}(K^-, \pi^-)_{\Lambda}^{12}\text{C}^*$. The validity of the approximation (3.2) deserves further study, however.

With the simplifications of Eqs. (3.1) and (3.2), the differential cross section in the laboratory system for the formation of a Λ particle, neutron hole state of the residual hypernucleus in the reaction $^A Z(\pi^+, K^+)_{\Lambda}^A Z^*(J^\pi)$ is given by

$$\frac{d\sigma}{d\Omega}(0^\circ \rightarrow J^\pi) = \alpha \left(\frac{d\sigma}{d\Omega} \right)_{L, 0^\circ}^{\pi^+ n \rightarrow K^+ \Lambda} \sum_{J_z} |M_{i_{\Lambda} j_{\Lambda} i_n j_n}^{J, J_z}|^2. \quad (3.3)$$

In Eq. (3.3), we have assumed a 0^+ closed shell target, and labeled the shell model state of the Λ by $\{i_{\Lambda}, j_{\Lambda}\}$ and that of the neutron hole by $\{i_n, j_n\}$. If configuration mixing of different particle-hole states of the same total angular momentum J and parity π is included, we replace M by $\sum_{i_{\Lambda} j_{\Lambda} i_n j_n} \alpha_{i_{\Lambda} j_{\Lambda} i_n j_n} M_{i_{\Lambda} j_{\Lambda} i_n j_n}^{J, J_z}$ in Eq. (3.3), where the weights $\alpha_{i_{\Lambda} j_{\Lambda} i_n j_n}$ are determined by diagonalization of the Hamiltonian, including the residual Λ -nucleon interaction. In the case of primary interest here, namely the stretch states of maximum spin, there is only one Λn^{-1} configuration available, so the

states are "pure." Note that even a pure $(\Lambda n^{-1})_J$ state can mix with a variety of two particle-two hole states $(\Lambda n_1 n_2^{-1} n_3^{-1})_J$, giving rise to a "spreading width" Γ_+ and a distribution of the strength of

the Λn^{-1} state over the more complicated excitations of the system.

The amplitude M in Eq. (3.3) can be cast in the form

$$M_{i_\Lambda j_\Lambda i_n j_n}^{J, J_Z} = \frac{1}{(2\pi)^6} (-1)^{J+J_Z+j_n-1/2} [(2J+1)(2j_\Lambda+1)(2j_n+1)]^{1/2} \begin{pmatrix} j_\Lambda & j_n & J \\ \frac{1}{2} & -\frac{1}{2} & 0 \end{pmatrix} \\ \times \sum_{i_a, i_b} i^{i_b-i_a} (2l_a+1)(2l_b+1) \begin{pmatrix} J & l_a & l_b \\ 0 & 0 & 0 \end{pmatrix} \begin{pmatrix} J & l_a & l_b \\ -J_Z & 0 & J_Z \end{pmatrix} \hat{Y}_{i_b, J_Z}(\Omega_f) \\ \times \sum_{n, n'} a_{n i_a} a_{n' i_b} \int_0^\infty r^2 dr R_{i_n j_n}(r) R_{i_\Lambda j_\Lambda}(r) j_{i_b}(k_n, r) j_{i_a}(k_n, r), \quad (3.4)$$

where $l_\Lambda + l_n + J$ must be even (natural parity only). Here we have picked the Z axis along the initial beam direction and Ω_f is the solid angle of the outgoing kaon. The sums over l_a and l_b represent the partial wave expansions for the initial pion and final kaon, respectively. The sums over n and n' correspond to the expansion of distorted partial waves in a plane wave basis. For $\{k_n\}$, we choose 11 momenta centered around the incident $k_{\pi L}$, with intervals of 50 MeV/c. For $\{k_{n'}\}$, the central momentum is k_{K^+L} . The function \hat{Y} is defined by

$$\hat{Y}_{i_b, J_Z}(\Omega_f) \equiv Y_{i_b, J_Z}(\Omega_f) (4\pi/2l_b+1)^{1/2}, \quad (3.5)$$

while the radial wave functions $R(r)$ are normalized according to

$$\int_0^\infty r^2 dr R^2(r) = 1. \quad (3.6)$$

Comparing Eq. (3.3) to (2.7), we see that the effective neutron number N_{eff}^J is given by

$$N_{\text{eff}}^J = \sum_{J_Z} |M_{i_\Lambda j_\Lambda i_n j_n}^{J, J_Z}|^2. \quad (3.7)$$

Note that the angular dependence of N_{eff}^J is carried by the factors $\hat{Y}_{i_b, J_Z}(\Omega_f)$ in Eq. (3.4). For $\theta_L = 0^\circ$, Eqs. (3.3), (3.4), and (3.7) reduce to the expressions given in Ref. 17, if we in addition set $\alpha = 1$, which is valid for (K^-, π^-) reactions with $q \approx 0$. As a further check on Eq. (3.7), one may neglect distortion effects, i.e., $a_{n i_a} = \delta_{k_n, k_{\pi L}}$, $a_{n' i_b} = \delta_{k_{n'}, k_{K^+L}}$, and use the identity (here for $\theta_L = 0^\circ$):

$$i^J j_J(qr) = \sum_{i_a, i_b} i^{i_b-i_a} j_{i_b}(k_{K^+L} r) j_{i_a}(k_{\pi L} r) \begin{pmatrix} l_a & l_b & J \\ 0 & 0 & 0 \end{pmatrix}^2 \\ \times (2l_a+1)(2l_b+1), \quad (3.8)$$

where $q = k_{\pi L} - k_{K^+L}$. We then obtain the plane wave approximation¹⁷

$$N_{\text{eff}}^J = (2J+1)(2j_\Lambda+1)(2j_n+1) \begin{pmatrix} j_\Lambda & j_n & J \\ \frac{1}{2} & -\frac{1}{2} & 0 \end{pmatrix}^2 F(q), \quad (3.9)$$

where $l_n + l_\Lambda + J$ is even, and

$$F(q) = \left(\int_0^\infty r^2 dr R_\Lambda(r) R_n(r) j_J(qr) \right)^2. \quad (3.10)$$

The pion and kaon distorted waves were generated by using a standard optical potential $V(r)$ of the form

$$-2EV(r) = k_L^2 b_0 \rho(r) - b_1 \vec{\nabla} \cdot \rho(r) \vec{\nabla}, \quad (3.11)$$

where $\rho(r)$ is normalized to the total number of nucleons A , $E = (\mu^2 + k_L^2)^{1/2}$ is the total laboratory energy, and the complex constants b_i (in fm³) are obtained from spin-isospin averaged s and p -wave elementary amplitudes.

The DWIA calculations reported in Sec. V were done for two typical incident momenta $p_{\pi L} = 1.04$ and 1.515 GeV/c, where the $\pi^+ n \rightarrow K^+ \Lambda$ cross sections have been measured.¹⁴ The target was taken to be ⁴⁰Ca, represented by a density

$$\rho(r) = \rho_0 / (1 + e^{(r-R)/a}), \quad (3.12)$$

with $R = 3.67$ fm and $a = 0.6$ fm. Using many-body kinematics to obtain the final momentum p_{KL} and the kinetic energies $T_{\pi L}$ and T_{KL} at 0° we have

$$p_{\pi L} = 1.04 \text{ GeV/c}, \quad T_{\pi L} = 910 \text{ MeV}, \quad (3.13a)$$

$$p_{KL} = 0.72 \text{ GeV/c}, \quad T_{KL} = 378 \text{ MeV}$$

and

$$p_{\pi L} = 1.52 \text{ GeV/c}, \quad T_{\pi L} = 1382 \text{ MeV}, \quad (3.13b)$$

$$p_{KL} = 1.25 \text{ GeV/c}, \quad T_{KL} = 851 \text{ MeV},$$

corresponding to $q \approx 0.32$ and 0.265 GeV/c, respectively. Note that q is the momentum transfer to the nucleus; a substantially larger value is obtained if one uses (inappropriately) two-body kinematics.

Consider the kinematics of Eq. (3.13a) first. Here the final state kaon emerges in a momentum region where the elementary K^*N s and p wave amplitudes dominate. The exotic Z_0^* resonance in the $P_{1/2}$, $I=0$ channel is starting to develop and partial waves with $l \geq 2$ are negligible. The Kisslinger form (3.11) is then a reasonable first guess for the K^* optical potential. We use the K^*N amplitudes of Martin²² to obtain

$$\begin{aligned} b_0 &= -0.326 + 0.228i \text{ fm}^3, \\ b_1 &= 0.089 + 0.145i \text{ fm}^3, \end{aligned} \quad (3.14)$$

for $k_{KL} = 0.72 \text{ GeV}/c$.

For Eq. (3.13b), the situation is somewhat different. In addition to the presence of a possible exotic Z_1^* resonance in the $P_{3/2}$, $I=1$ channel for K^*N , there are also significant contributions from d and f waves. We still isolate the p -wave part of $V(r)$ as in Eq. (3.11) but we lump the $l \geq 2$ partial waves together with the $l=0$ part to make up an "effective" value

$$\text{Im } b_0^{\text{eff}} = (\langle \sigma_{\text{TOT}} \rangle_{\text{AV}} - \langle \sigma_{l=1} \rangle) / k_{KL}, \quad (3.15)$$

where $\langle \sigma_{\text{TOT}} \rangle_{\text{AV}} = \frac{1}{2}(\sigma_{K^*p} + \sigma_{K^*n})$ and $\langle \sigma_{l=1} \rangle = k_{KL} \text{Im } b_1$. We still retain the s -wave estimate for $\text{Re } b_0$, which is small in any case. Using the Martin²² amplitudes, we get

$$\begin{aligned} b_0^{\text{eff}} &= -0.085 + 0.173i \text{ fm}^3, \\ b_1 &= 0.0013 + 0.132i \text{ fm}^3, \end{aligned} \quad (3.16)$$

for $k_{KL} = 1.25 \text{ GeV}/c$.

To construct a rough approximation to the pion optical potential for momenta $\geq 1 \text{ GeV}/c$, where a number of partial waves contribute, we use experimental information on total πN cross sections²³ and the real parts of $\pi^\pm p$ forward scattering amplitudes²⁴ rather than partial wave analyses. Thus we use a local optical potential with $b_1 = 0$, and we obtain b_0 from

$$\text{Re } b_0 = \frac{1}{2k_{rL}} (\alpha_n \sigma_{\pi^+n} + \alpha_p \sigma_{\pi^+p}), \quad (3.17)$$

$$\text{Im } b_0 = \langle \sigma_{\text{TOT}} \rangle_{\text{AV}} / k_{rL},$$

where $\alpha_{n,p} = \text{Re } f_{\pi^+n,p} / \text{Im } f_{\pi^+n,p}$.

Near $k_{rL} = 1.04 \text{ GeV}/c$, the real amplitudes α are very small and $\langle \sigma_{\text{TOT}} \rangle_{\text{AV}} \approx 40 \text{ mb}$, so we use

$$b_0 \approx 0.76i \text{ fm}^3. \quad (3.18)$$

In the region of $k_{rL} = 1.515 \text{ GeV}/c$, we have²⁴ $\alpha_n \approx -0.15$, $\alpha_p \approx -0.22$, and $\langle \sigma_{\text{TOT}} \rangle_{\text{AV}} \approx 38 \text{ mb}$. Using an average value $\alpha \approx -0.18$, we obtain

$$b_0 = -0.087 + 0.484i \text{ fm}^3. \quad (3.19)$$

In both cases, the real part of b_0 is not well determined. However, for the (K^-, π^-) reaction,²⁰ it

has been shown that the results are quite insensitive to the choice of $\text{Re } b_0$ since the absorptive part of the pion optical potential is strong. Note that in the presence of resonances in the elementary amplitudes, the first order optical potential (3.11) is in any event a very crude approximation.

The bound state radial wave functions $R(r)$ of Eq. (3.4) for the Λ and neutron hole in ${}^{40}_{\Lambda}\text{Ca}$ have been generated for both harmonic oscillator and Woods-Saxon potentials. The same oscillator parameter $b = 2.03 \text{ fm}$ was taken for both Λ and n^{-1} states; the wave functions are given by Eq. (4.1). The particular high spin stretch configurations we consider in ${}^{40}_{\Lambda}\text{Ca}$ are the following:

$$\begin{aligned} &({}_{\Lambda}p_{3/2} \otimes {}_n d_{3/2}^{-1})_{3-}, \\ &({}_{\Lambda}d_{5/2} \otimes {}_n d_{3/2}^{-1})_{4+}, \\ &({}_{\Lambda}f_{7/2} \otimes {}_n d_{3/2}^{-1})_{5-}. \end{aligned} \quad (3.20)$$

The $d_{3/2}^{-1}$ neutron hole is taken to have a binding energy of 15.63 MeV, the separation energy of a neutron in ${}^{40}\text{Ca}$. We fit this binding energy with a central Woods-Saxon potential of form (4.4) with $V_0 = 52.9 \text{ MeV}$, $R = 4.24 \text{ fm}$, $a = 0.6 \text{ fm}$, and a Thomas spin-orbit potential of strength $V_{s_0} = 6 \text{ MeV}$. For the Λ , we use the same values of R and a , but set $V_{s_0} = 0$ and adjust V_0 to produce binding energies of 9, 0.5, and 0.1 MeV for the ${}_{\Lambda}p_{3/2}$, ${}_{\Lambda}d_{5/2}$, and ${}_{\Lambda}f_{7/2}$ states, respectively. This requires depths $V_0 = 24.64, 22.63, \text{ and } 36.94 \text{ MeV}$. The binding energies for the ${}_{\Lambda}p_{3/2}$ and ${}_{\Lambda}d_{5/2}$ states are suggested by the CERN data on ${}^{40}\text{Ca}(K^-, \pi^-){}_{\Lambda}\text{Ca}^*$, reviewed in Ref. (25). The true ${}_{\Lambda}f_{7/2}$ state lies at about 5 MeV in the continuum (see Fig. 6 and Ref. 25); for numerical convenience we have replaced it by a bound state with essentially zero binding. The use of a proper continuum wave function for ${}_{\Lambda}f_{7/2}$ would lead to some further modest decrease of the cross section to the $({}_{\Lambda}f_{7/2} \otimes {}_n d_{3/2}^{-1})_{5-}$ state with respect to the estimate given here. The actual results of the calculation are presented and discussed in Sec. V.

B. Eikonal distortions

In the preceding section we outlined the procedure associated with a partial wave decomposition of the DWIA. Unfortunately this procedure, for high momentum processes, tends to become computationally lengthy due to the large number of partial waves required. Thus there is motivation to pursue a somewhat simpler procedure; i.e., the use of eikonal generated distortions.²⁶ The primary function of the distorted waves is to remove flux from the nuclear interior, thus any reasonable optical potential which has the appropriate strength should yield qualitatively accept-

able results. Quantitatively we expect the results to be of the right magnitude and different final states to have the correct relative strengths. Later in this paper we compare the results obtained using fully distorted waves and those obtained using the eikonal approximation.

We first specify the eikonal distorted waves $\chi^{(\pm)}$. These are obtained from a complex energy dependent potential defined by

$$U_m(r) = \frac{-4\pi(\hbar c)^2}{2E_L} \{f(0)_{mn} \rho_n(r) + f(0)_{mp} \rho_p(r)\}. \quad (3.21)$$

Here $f(0)_{mn}$ and $f(0)_{mp}$ are the lab forward elementary amplitudes for meson-neutron and meson-proton scattering respectively; ρ_n and ρ_p are the neutron and proton densities normalized such that $\int \rho_n d^3r = N$ and $\int \rho_p d^3r = Z$. E_L is the total meson lab energy. By use of the optical theorem, the scattering amplitudes may be related to the meson-nucleon total cross sections; thus

$$f(0) = i\bar{\sigma} k_L / 4\pi, \quad (3.22)$$

where k_L is the meson lab momentum, $\bar{\sigma} = \sigma^{\text{TOT}}(1 - i\gamma)$, and $\gamma = \text{Re} f(0) / \text{Im} f(0)$. The eikonal phase shift functions $\xi^{(\pm)}(\vec{r})$ are generated from the optical potential by

$$\xi_m^{(+)}(\vec{r}) = -\frac{1}{\hbar v} \int_{-\infty}^Z U_m(b, Z') dZ' \quad (3.23a)$$

and

$$\xi_m^{(-)}(\vec{r}) = -\frac{1}{\hbar v} \int_Z^{\infty} U_m(b, Z') dZ'. \quad (3.23b)$$

Here the index m denotes the meson and meson-nucleus optical potential.

The eikonal distorted waves can now be written as

$$\langle \vec{r} | \chi_{m\vec{p}}^{(+)} \rangle = \exp[i\vec{p} \cdot \vec{r} + i\xi_m^{(+)}(\vec{r})] \quad (3.24a)$$

and

$$\langle \chi_{m\vec{p}}^{(-)} | \vec{r} \rangle = \exp[-i\vec{p} \cdot \vec{r} + i\xi_m^{(-)}(\vec{r})]. \quad (3.24b)$$

In order to simplify the notation in the following development we assume that the proton and neutron density distributions are equal and define an isospin averaged meson-nucleon effective cross section $\bar{\sigma}_m$ as follows:

$$\bar{\sigma}_m = (Z/A)\bar{\sigma}_{mp} + (N/A)\bar{\sigma}_{mn}. \quad (3.25)$$

Tables I and II list typical values of pion-nucleon total cross sections and kaon-nucleon total cross sections for various momenta. Values of γ are not given as these quantities are not well determined. The differential cross section are insensitive ($\sim 4\%$) to wide variation ($-1 \lesssim \gamma \lesssim 1$) in the

TABLE I. Pion-nucleon total cross sections.

Projectile	Momentum (GeV/c)	$\sigma^{\text{TOT}}(\pi^+, p)^a$ (mb)	$\sigma^{\text{TOT}}(\pi^+, n)^b$ (mb)
π^+	1.02	25.2	58.5
	1.04	26.1	55.2
	1.097	23.8	45.7
	1.159	28.0	40.2
	1.225	31.0	36.8
	1.289	35.0	36.1
	1.334	38.1	36.6
	1.395	36.7	35.7
	1.455	41.6	36.3
	1.515	40.1	35.1
	1.575	39.5	35.0
1.645	39.1	34.1	
π^-		$\sigma^{\text{TOT}}(\pi^-, p)^c$	$\sigma^{\text{TOT}}(\pi^-, n)^d$
	0.40	31.9	
	0.51	26.8	31.2
	0.58	28.0	23.8
	0.67	39.9	16.1
	0.75	46.0	15.7
	0.84	37.9	16.9
	0.93	43.0	23.0

^a Values from Compilation of cross sections I: π^- and π^+ induced reactions, Report No. CERN/HERA 72-1.

^b By using charge independence, the values of $\sigma(\pi^+ n)$ are related to the value of $\sigma(\pi^- p)$. These values are obtained from footnote a.

^c Values from footnote a.

^d By using charge independence, the values of $\sigma(\pi^-, n)$ are related to the values of $\sigma(\pi^+, p)$. These values are obtained from footnote a.

value of γ . We now define

$$T(b) \equiv \int_{-\infty}^{\infty} \rho(r) dZ, \quad (3.26)$$

such that $\int T(b) d^2b = A$, and a nuclear defect function $D(b, Z)$ by

$$\begin{aligned} D(b, Z) &\equiv \int_{-\infty}^Z \rho(r) dZ' - \int_Z^{\infty} \rho(r) dZ' \\ &= 2 \int_0^Z \rho(b, Z') dZ'. \end{aligned} \quad (3.27)$$

Adopting these definitions we express the product of the distorted waves as

$$\langle \chi_{m\vec{p}_f}^{(-)} | \vec{r} \rangle \langle \vec{r} | \chi_{m\vec{p}_i}^{(+)} \rangle = \exp\left(i\vec{q} \cdot \vec{r} - \frac{\sigma}{2} T(b) - \frac{\Delta}{2} D(b, Z)\right). \quad (3.28)$$

Here $\vec{q} = \vec{p}_i - \vec{p}_f$ is the momentum transfer, $\sigma = (\bar{\sigma}_{m_i} + \bar{\sigma}_{m_f})/2$ is the mean meson-nucleon effective cross section, and $\Delta = (\bar{\sigma}_{m_i} - \bar{\sigma}_{m_f})/2$ is the cross section defect function. Consider the term $\exp[-(\Delta/2)D(b, Z)]$; this differs from unity only for values of b small compared to the nuclear size.

TABLE II. Kaon-nucleon total cross section.

Projectile	Momentum (GeV/c)	$\sigma^{\text{TOT}}(K^+, p)^a$ (mb)	$\sigma^{\text{TOT}}(K^+, n)^b$ (mb)
K^+	0.50	12.6	12.5
	0.61	12.3	14.3
	0.71	11.1	16.5
	0.82	13.2	16.4
	0.92	14.2	17.2
	1.02	16.1	18.5
	1.055	17.0	18.9
	1.125	17.6	19.6
	1.207	19.9	20.3
	1.30	17.9	19.4
	1.40	18.0	19.2
	1.55	17.7	18.9
1.70	17.7	18.8	
K^-		$\sigma^{\text{TOT}}(K^-, p)^c$	$\sigma^{\text{TOT}}(K^-, n)^d$
	0.50	43.5	20.0
	0.60	37.5	26.2
	0.70	33.1	31.0
	0.80	40.2	30.0
	0.90	43.4	35.0
	1.00	49.5	38.0
	1.10	44.0	36.0

^a Values from (i) Compilation of cross sections II: K^- and K^+ induced reactions, Report No. CERN/HERA 75-1; (ii) A compilation of K^-N cross sections below 2 GeV/c, Report No. CERN/HERA 75-1.

^b Values estimated from expression $\sigma(K^+n) \approx \sigma(K^+D) - \sigma(K^+p)$. Cross sections obtained from footnotes a (i) and a (ii).

^c Values from footnote a (i).

^d Values estimated from expression $\sigma(K^-n) \approx \sigma(K^-D) - \sigma(K^-p)$ and footnote a (i).

$$\{JJ_Z; l_\Lambda m_\Lambda j_\Lambda; l_n m_n j_n\} = (-)^{j_n + l_n + l_\Lambda + 1/2 + m_\Lambda} [(2J+1)(2j_\Lambda+1)(2j_n+1)]^{1/2}$$

$$\times \begin{Bmatrix} l_n & l_\Lambda & J \\ -m_n & m_\Lambda & -J \end{Bmatrix} \begin{Bmatrix} l_n & l_n & J \\ j_\Lambda & j_n & \frac{1}{2} \end{Bmatrix} \quad (3.32)$$

Following the techniques used by Ludeking [Ref. 27], Eq. (3.31) may be reduced to a completely analytic form by using harmonic oscillator wave functions and expressing the distortion factor $E(b)$ by a sum of Gaussians with complex weights; i.e.,

$$E(b) \approx 1 + \sum_{s=1}^{s_{\max}} c_s \exp(-\alpha_s b^2). \quad (3.33)$$

It was found that typically $s_{\max} = 6$ was adequate to represent $E(b)$ within a few percent over the range of b for which $E(b)$ differed significantly from unity. Parenthetically, we note that the restriction to harmonic oscillator wave functions is not as severe as might be expected, since it is a

Thus its effects are limited to the nuclear interior, which should be relatively unimportant for forward angle scattering studies of strongly absorbed particles. Hence for current purposes we shall replace this factor by unity. Therefore we approximate Eq. (3.28) by

$$\langle \chi^{(-)} | \bar{\mathbf{r}} \rangle \langle \bar{\mathbf{r}} | \chi^{(+)} \rangle \approx \exp(i\vec{q} \cdot \bar{\mathbf{r}}) E(b), \quad (3.29)$$

where the distortions of the mesons have been reduced to a complex form factor $E(b) = \exp[-\sigma T(b)/2]$ which simulates the absorptivity of the nuclear medium.

We may reexpress M [see Eq. (3.4)] in the eikonal approximation as

$$M_{l_\Lambda j_\Lambda l_n j_n}^{JJ_Z} \approx \sum_{m_\Lambda m_n} \{\text{spin-angle-coupling}\} \times \int d^3r \exp(i\vec{q} \cdot \bar{\mathbf{r}}) E(b) \Phi_\Lambda^*(\bar{\mathbf{r}}) \Phi_n(\bar{\mathbf{r}}). \quad (3.30)$$

We then write the effective neutron number N_{eff}^J as

$$N_{\text{eff}}^J = \sum_{J_Z} |M_{l_\Lambda j_\Lambda l_n j_n}^{JJ_Z}|^2, \quad (3.31)$$

which may be compared with Eq. (3.7). As before we have assumed a single lambda-particle neutron-hole configuration coupled to a total angular momentum (JJ_Z). Here the Φ 's are configuration space wave functions of the participating baryons and the indices Λ and N denote all necessary remaining quantum numbers. The curly bracket includes all the spin-angle coupling to JJ_Z . Explicitly this is written as

simple extension to represent more realistic single particle wave functions by an expansion in the harmonic oscillator basis. Results obtained using the approximations described here for eikonal distortions are discussed in Sec. V.

C. The Quasielastic response function

The nuclear response function has a quasifree contribution as well as a bound state spectrum. This process corresponds to the production of a free Λ and thus threshold for the contribution occurs when $B_\Lambda = 0$. If the baryons were independent and at rest, one would anticipate a peak at an energy loss given by the free kinematics of

$$\omega_{\text{free}} = q^2/2M_\Lambda + M_\Lambda - M_n. \quad (3.34)$$

Using a simple Fermi-gas model, an individual nucleon is characterized by a momentum distribution up to the Fermi-momentum K_F , the nucleon being in an averaged momentum independent single particle potential U . The physical result in such a model is that the peak of the response function is displaced on the energy scale and has a finite width characterized by q , the momentum transfer. Using energy conservation the energy loss defined by $\omega \equiv E_{m_i} - E_{m_f}$, may also be expressed as

$$\begin{aligned} \omega = & M_\Lambda - M_N + U_N - U_\Lambda - P_N^2/2M_N \\ & + (\vec{P}_N + \vec{q})^2/2M_\Lambda, \end{aligned} \quad (3.35)$$

where $\vec{q} = \vec{p}_{m_i} - \vec{p}_{m_f}$. (The indices m_i and m_f denote the incident and scattered mesons, respectively.)

Considering the nucleus as a Fermi gas, in which each nucleon moves freely in the field of a uniform nuclear potential U , the differential cross section may be written as

$$\frac{d^2\sigma}{d\Omega_2 d\epsilon_2} = \alpha \frac{d\sigma}{d\Omega} (\text{elem}) R(Q, \nu). \quad (3.36)$$

The response function $R(Q, \nu)$ is defined by

$$\begin{aligned} R(Q, \nu) = & \frac{3\tilde{N}_{\text{eff}}}{4\pi K_F^3} \int d^3P_N \theta(K_F - P_N) \\ & \times \delta(K_F^2/M_\Lambda (\nu + \alpha^2 k - k \cdot Q - Q^2/2)), \end{aligned} \quad (3.37)$$

where $k = P_N/K_F$, $Q = q/K_F$, $\alpha^2 = (M_\Lambda - M_N)/2M_N$, and

$$\nu = [\omega - (M_\Lambda - M_N) - (U_N - U_\Lambda)] / (K_F^2/M_\Lambda). \quad (3.38)$$

The inclusion of \tilde{N}_{eff} in Eq. (3.37) constitutes a somewhat *ad hoc*, although plausible, procedure. Equation (3.37) differs from the usual quasielastic response function studied in, for example, inelastic electron scattering, because the final free Λ does not have to be above the Fermi sea, its mass differs from that of the neutron, and finally the average single particle potential it experiences is considerably weaker than that of the initial neutron.²⁸

The quantity \tilde{N}_{eff} refers to the effective number of neutrons present in the Fermi gas. Since absorption occurs in both the entrance and exit channels, the effective number of neutrons is reduced and $\tilde{N}_{\text{eff}} < N$. In the framework of the distorted wave formulation \tilde{N}_{eff} may be approximated by²⁸

$$\tilde{N}_{\text{eff}} \approx \int d^3r \rho_N(r) |\chi_{\vec{p}_f}^{(-)}(r)|^2 |\chi_{\vec{p}_i}^{(+)}(r)|^2. \quad (3.39)$$

Within the context of the eikonal approximation al-

ready described this becomes

$$\tilde{N}_{\text{eff}} \approx \int d^2b T_N(b) \exp[-\text{Re}\sigma T_A(b)], \quad (3.40)$$

which in the limit of no absorption ($\sigma \rightarrow 0$) reduces to the actual neutron number. [$T_N(b)$ and $T_A(b)$ are the neutron and nuclear thickness functions.]

Evaluating the function $R(Q, \nu)$ leads to

$$(1) \quad Q > 2\alpha^2; Q^2/2 - Q - \alpha^2 \leq \nu \leq Q^2/2 + Q - \alpha^2:$$

$$R = \frac{3M_\Lambda \tilde{N}}{4QK_F^2} \left(1 - \frac{1}{4\alpha^4} \{Q - [Q^2 - 4\alpha^4(\nu - Q^2/2)]^{1/2}\}^2 \right), \quad (3.41a)$$

$$(2a) \quad 0 < Q < 2\alpha^2; Q^2/2 - Q - \alpha^2 \leq \nu \leq Q^2/2 + Q - \alpha^2:$$

$$R = \frac{3M_\Lambda \tilde{N}}{4QK_F^2} \left(1 - \frac{1}{4\alpha^4} \{Q - [Q^2 - 4\alpha^2(\nu - Q^2/2)]^{1/2}\}^2 \right), \quad (3.41b)$$

$$(2b) \quad 0 < Q < 2\alpha^2; Q^2/2 + Q - \alpha^2 \leq \nu \leq Q^2/2(1 + \frac{1}{2}\alpha^2):$$

$$R = \frac{3M_\Lambda \tilde{N}}{4K_F^2} [Q^2 - 4\alpha^2(\nu - Q^2/2)]^{1/2} / \alpha^4. \quad (3.41c)$$

These formulas reduce to those of Dalitz and Gal²⁸ for small Q ; these authors first evaluated the quasielastic spectrum for the (K^-, π^-) reaction. In Fig. 4 the qualitative behavior of $R(Q, \nu)$ is displayed. Note that for small values of Q , the response function has a pronounced peak. This behavior suggests that for very small momentum transfer processes it is possible to misidentify a quasifree peak as a "p-h" bound state in the continuum. For the (K^-, π^-) reaction this is certainly a consideration, since the initial attractiveness of that process included the possibility of producing low spin substitutional states in which the lambda was created at "rest" in the nucleus (i.e., at forward angles the momentum transfer is quite small). Alternatively for the (π^+, K^+) processes, this possibility is obviated by the fact that the threshold beam momentum yields a momentum transfer $q \approx K_F$ and decreases rather slowly with increasing beam energy. From Eqs. (3.41a)–(3.41c) it is apparent that the width of the quasifree response is proportional to Q and height varies approximately as $1/Q$. Since experiments are typically carried out at fixed angle θ , we display in Fig. 5 the type of trajectory the response function follows in the (Q, ν) plane. For physical nuclei, the continuum threshold point does not occur at $R(Q, \nu) = 0$ for the Fermi gas model. Detailed results including the quasielastic response for selected nuclei are discussed in Sec. V.

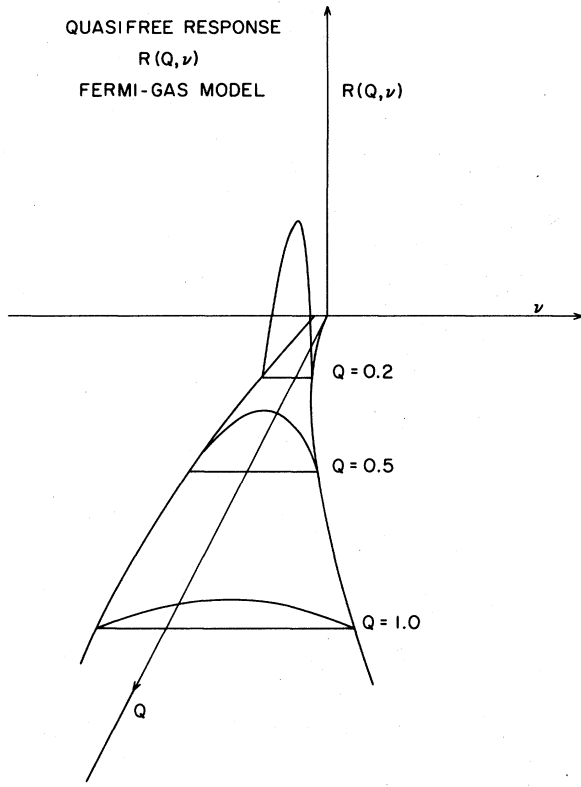


FIG. 4. Schematic description of the quasifree response function $R(Q, \nu)$ in terms of the dimensionless variables Q and ν . Normalization is arbitrary, the relative height reflects the functional behavior in the Q - ν plane. The variable Q is the momentum transfer in units of the Fermi momentum K_F . The symbol ν is a dimensionless energy variable.

IV. EXCITATION OF HIGH SPIN STATES IN THE (π, K) REACTION

The essential physical features of high momentum transfer processes can be understood in the plane wave approximation (PWA). The effect of optical potential distortions of the π^+ and K^+ waves is merely to reduce the cross sections in PWA by about an order of magnitude, leaving the angular shape almost unchanged. We include distorting potentials in the quantitative results presented in Sec. V. In the present section, we use oscillator wave functions to describe the Λ particle and neutron hole states. This enables us to obtain closed form results which exhibit the physics of the problem. For more quantitative estimates, particularly for Λ orbits which are loosely bound or in the continuum, we use wave functions generated by a Woods-Saxon potential, which has a more realistic behavior in the nuclear surface. We compare calculations with Woods-Saxon and oscillator wells in

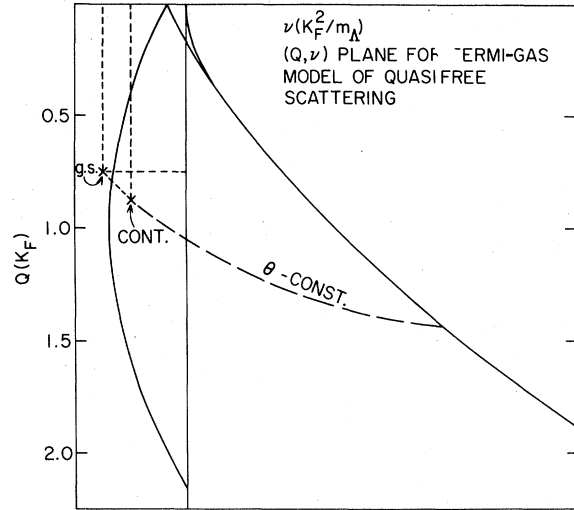


FIG. 5. For the Fermi-gas model of quasifree scattering, we show the trajectory in the (Q, ν) plane that the quasielastic spectrum would follow for constant scattering angle θ . Note that the true continuum point will not coincide with the zero of the Fermi-gas quasifree response function.

a later section.

Since $q > K_F$ for the (π^+, K^+) reaction, it is clear that high spin states of the residual hypernucleus will be preferentially populated. This crucial point was not emphasized in several preliminary estimates.²⁹ To see this explicitly, consider a *natural parity* "stretch configuration" of spin $J = l_\Lambda + l_n$ obtained by coupling Λ in shell model orbit $(l_\Lambda j_\Lambda)$ to a neutron hole in orbit $(l_n j_n)$. The effective neutron number N_{eff}^J , related to the 0° (π^+, K^+) cross section via Eq. (2.7), is given by Eqs. (3.9) and (3.10). Note that $F(q)$ appearing in (3.9) is the *form factor* which carries the dependence on momentum transfer. For an oscillator potential of radius parameter b , we have

$$R_l(r) = c_l (r/b)^l e^{-r^2/2b^2} \quad (4.1)$$

for nodeless states ($n=1$), where $c_l = [2^{l+2}/b^3 \sqrt{\pi} (2l+1)!!]^{1/2}$. For natural parity stretch states ($J = l_\Lambda + l_n$), we have

$$F(q) = \frac{(2Z)^J e^{-Z}}{[(2J+1)!!]^2 \Gamma(l_\Lambda + 3/2) \Gamma(l_n + 3/2)}, \quad (4.2)$$

with $Z = (bq)^2/2$. Note that we consider only natural parity states, since we will be mainly interested in (π^+, K^+) cross sections at 0° ; the cross sections to unnatural parity states depend on spin-flip $\pi^+ n \rightarrow K^+ \Lambda$ amplitudes, which vanish identically at 0° . Calculations of the (K^-, π^-) cross sections

at finite angle to unnatural parity states²⁰ indicate very small peak cross sections relative to those for natural parity states of the same J . We expect a similar result for (π^+, K^+) reactions.

In Fig. 6, we display the form factor $F(q)$ for a transition to the $(\Lambda p_{1/2, 3/2} \otimes \pi p_{3/2}^{-1})_{2^+}$ states of ^{12}C . Note that $F(q)$, which gives the shape of the angular distribution for the excitation of these states in PWA, is the *same* function for (K, π) and (π, K) reactions. The only difference is that $\theta_L = 0^\circ$ corresponds to quite different values of q for the two cases. This is indicated in Fig. 6. The (K^-, π^-) reaction displays a sharp peak at $\theta_L = 15^\circ$ for the excitation of the 2^+ . In the (π^+, K^+) reaction, on the other hand, $\theta_L = 0^\circ$ corresponds to large q , so we are seeing only the tail region of $F(q)$. By shifting the (K^-, π^-) angular distribution to the right, it will overlap exactly with the (π^+, K^+) distribution, i.e., $(d\sigma/d\Omega)^{(\pi, K)}$ for $\theta_L \geq 20^\circ$ corresponds (except for the ratio of the associated elementary cross sections) to $(d\sigma/d\Omega)^{(K, \pi)}$ for $\theta_L \geq 0^\circ$ in PWA.

For the (K^-, π^-) process, we can always see the peak of $F(q)$ by looking at an appropriate finite θ_L (which increases with J). For (π^+, K^+) , this is

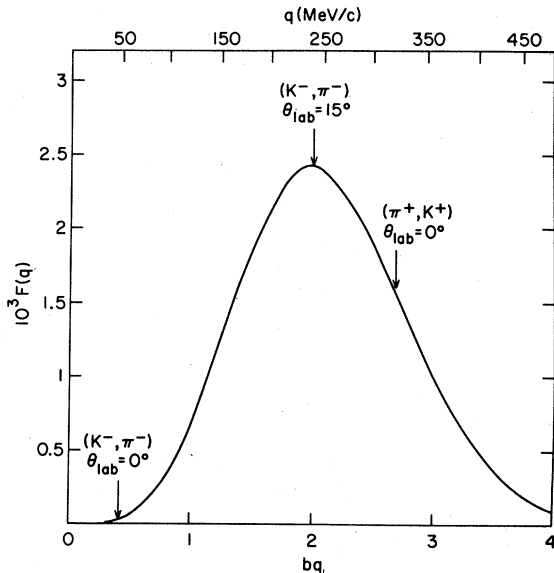


FIG. 6. The form factor $F(q)$ of Eq. (3.10) for a transition from the 0^+ ground state of a ^{12}C target to the $(\Lambda p_{3/2} \otimes \pi p_{3/2}^{-1})_{2^+}$ state of the residual hypernucleus $^{12}\text{C}^*$, excited by either the (K^-, π^-) or (π^+, K^+) reaction. The top scale shows the value of q , assuming $b = 1.64$ fm. The values of q corresponding to $\theta_L = 0^\circ$ are indicated by arrows for (K, π) and (π, K) reactions, as well as $\theta_L = 15^\circ$ for (K, π) , corresponding to the peak cross section. To make the correspondence between q and θ_L , we have assumed $p_K \approx 800$ MeV/c and $p_\pi \approx 1.04$ GeV/c.

usually not true, since we are well past the maximum of $F(q)$, even for $\theta_L = 0^\circ$. In many cases, particularly for low spin final states, we are far out in the tail of $F(q)$, so the cross section is very small. There are cases, however, where $\theta_L = 0^\circ$ for (π, K) corresponds precisely to the peak of $F(q)$. This is the *optimal matching* of q and J . For stretch configurations, this occurs when

$$J = (bq)^2/2. \quad (4.3)$$

The states of optimum J given by Eq. (4.3) will dominate the (π, K) cross section. Assuming the rough variation $b \approx b_0 A^{1/3}$ with $b_0 \approx 0.6$ fm, we note that $J \sim A^{2/3}$. The dependence of J on A for various choices of p_π is illustrated in Fig. 7. Observe that as p_π increases, the value of q decreases and hence the optimum J also decreases. Thus by changing p_π , we are sensitive to a range of optimum J 's.

The crucial questions are now the following: What is the maximum J we can expect in a real hypernucleus? Can we achieve the optimum matching condition of Eq. (4.3)? The response to these questions depends on the spectroscopy of Λ single particle states in hypernuclei. We need to know the maximum orbital angular momentum l_Λ of Λ bound states or low-lying single particle resonances as a function of A . One could get some guidance on this point from the results of Hartree-Fock self-consistent calculations³⁰ for Λ hypernuclei. We adopt a more phenomenological

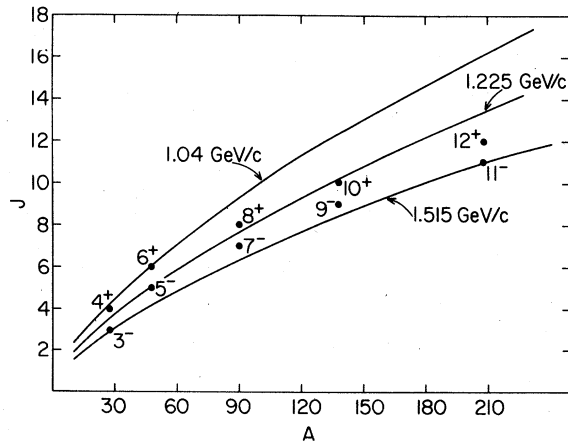


FIG. 7. Optimum J of Eq. (3.5) as a function of A for natural parity stretched configurations $(l_\Lambda \otimes l_n^{-1})_{J=l_\Lambda+l_n}$. The three solid curves correspond to three different incident pion momenta as labeled. The dots correspond to the available high spin states of Eqs. (4.5) and (4.6), labeled by J^π . Note that if one of the labeled J^π states lies above a solid line, the cross section to this state (at the momentum corresponding to the line) peaks at $\theta_L > 0^\circ$ rather than $\theta_L = 0^\circ$.

approach here, which assumes a Woods-Saxon form for the Λ single particle potential $V_\Lambda(r)$:

$$V_\Lambda(r) = -V_0/[1 + e^{(r-R)/a}], \quad (4.4)$$

with $R = r_0(A-1)^{1/3}$, $r_0 = 1.1$ fm, and $a = 0.6$ fm. Here $A-1$ is the number of nucleons (A = total baryon number). The depth V_0 is adjusted to produce the observed^{5,31} $s_{1/2}$ binding energy B_Λ of the Λ in $^{12}_\Lambda\text{C}$, which is $B_\Lambda(s_{1/2}) \approx -10.7$ MeV. This gives $V_0 = 30.7$ MeV. Using this same value for V_0 , we find that the $\Lambda p_{1/2,3/2}$ orbit is unbound by about 0.1 MeV; the experimental value⁵ is $B_\Lambda = 0.03 \pm 0.8$ MeV. Thus we do not require a spin-orbit potential for the Λ , consistent with the conclusions of the CERN group,³² and also the data of the BNL group,⁵ who did not observe any splitting (≥ 800 keV) of the configurations $(\Lambda p_{1/2} \otimes n p_{3/2}^{-1})_{2^+}$ and $(\Lambda p_{3/2} \otimes n p_{3/2}^{-1})_{0^+, 2^+}$ in $^{12}_\Lambda\text{C}$. The geometrical parameters of our Λ potential are the same as those used by Bouyssy,²¹ who adopted a somewhat smaller depth $V_0 \approx 28$ MeV.

Using a fixed value $V_0 = 30.7$ MeV for all A , and ignoring spin-orbit splittings, we have calculated the energies of Λ bound states and resonances for a variety of hypernuclei. Some of these results for B_Λ are given in Fig. 8. For Λ states in the continuum, we have obtained the single particle resonance energy $B_\Lambda = E_R$ from the condition $\delta(E_R) = \pi/2$, where $\delta(E)$ is the Λ -nucleus scattering phase shift due to the potential (4.4). The elastic width Γ , is obtained from the conventional formula $\Gamma = 2[d\delta(E)/dE]_{E=E_R}^{-1}$. The values of Γ , in MeV are included in parentheses in Fig. 8.

The hypernuclei included in Fig. 8 have the

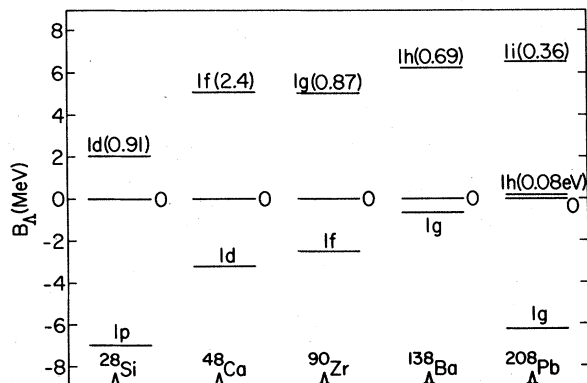


FIG. 8. Single particle binding energies B_Λ for a Λ in various shell model orbits in a hypernucleus. We show only the orbits closest to zero binding energy. $B_\Lambda > 0$ refers to Λ single particle resonances whose width (in parentheses) is given in MeV. The single particle potential of Eq. (4.4) was used and the spin-orbit term was neglected.

property that the corresponding nuclei ($\Lambda \rightarrow n$) have closed shells of neutrons with $j_n = l_n + \frac{1}{2}$ ($N = 14, 28, 50, 82,$ and 126). These are prime candidates for the formation of high spin states in the (π^+, K^+) reaction. From Fig. 8, we see that the Λ orbit with the same l value as the last bound shell of neutrons is *unbound*, typically by 5–6 MeV in heavier systems. Even though these Λ levels are in the continuum, the elastic widths Γ , remain fairly modest and thus the corresponding hypernuclear levels should still be observable. Note that the elastic width of these levels *decreases* rather sharply as we pass to large A , attaining a value of only $\Gamma, \approx 360$ keV for the $\Lambda i_{13/2}$ level in $^{208}_\Lambda\text{Pb}$. The main component of the observed width of hypernuclear configurations such as $(\Lambda i_{13/2} \otimes n i_{13/2}^{-1})_J$ may then be the spreading width Γ_s due to the mixing with 2 particle-2 hole states of the same J . However, for the Λn^{-1} states of maximum J considered here, the density of 2p2h states of spin J may be quite small and Γ_s will be less than for low J couplings of the same configuration. An additional contribution to the width can come from interaction of the Λ with a nucleon resulting in the ejection of the nucleon into the continuum with an accompanying transition of the Λ to a lower energy orbit (hypernuclear Auger effect).

For the nuclei shown in Fig. 8, we see that the natural parity states of maximum J which are likely to be observable consist of a Λ in the lowest-lying single particle resonance state coupled to a neutron hole in the same orbit, that is

$$[(l j_\Lambda) \otimes (l j_n)^{-1}]_{J=2l}, \quad (4.5)$$

where the states with $j_\Lambda = l \pm \frac{1}{2}$ are approximately degenerate in energy since the spin-orbit potential is weak. Configurations involving a Λ in the next highest resonant state (1g in $^{48}_\Lambda\text{Ca}$, for example) lead to one extra unit of J but are likely to be very broad ($\Gamma, > 5$ MeV). The states of maximum J involving a Λ in a *bound* orbit are of the form

$$[(l-1, j_\Lambda) \otimes (l j_n)^{-1}]_{J=2l-1}. \quad (4.6)$$

The configurations of Eq. (4.5) and (4.6) are indicated by dots in Fig. 7 for $^{28}_\Lambda\text{Si}$, $^{48}_\Lambda\text{Ca}$, $^{90}_\Lambda\text{Zr}$, $^{138}_\Lambda\text{Ba}$, and $^{208}_\Lambda\text{Pb}$. We note that in some cases the available high spin states lie very close to the optimum matching condition of Eq. (4.3). These states can be excited at $\theta_L = 0^\circ$ with the maximum possible cross section. For example, the 6^+ state in $^{48}_\Lambda\text{Ca}$, arising from $(\Lambda f_{5/2,7/2} \otimes n f_{7/2}^{-1})_{6^+}$, is optimally matched a $p_r = 1.04$ GeV/c, where the elementary cross section also peaks. The 5^- state in $^{48}_\Lambda\text{Ca}$ is well matched at a somewhat higher momentum of $p_r \approx 1.23$ GeV/c, and so forth. For heavier targets, good matching occurs at larger

values of p_π , for which the two body cross section has dropped well below its peak (see Fig. 2). Thus the optimum conditions for (π^+, K^+) experiments seem to exist for lighter targets ($A < 60$).

For the maximum J states of Eq. (4.5), the effective number of neutrons defined by Eq. (3.9) becomes

$$\sum_{j_\Lambda = l_\Lambda \pm 1/2} N_{\text{eff}}^{J=2l} = \beta_J Z^J e^{-Z}, \quad (4.7)$$

where $\beta_J = 2/9, 12/175, 32/14553, \text{ and } 4/104247$ for $J=2, 4, 6, \text{ and } 8$, respectively. The values of N_{eff} given by Eq. (4.7) are plotted in Fig. 9. We observe that N_{eff} is not a strong function of p_π , except possibly for ^{12}C . Note also that N_{eff} remains small (≤ 0.5) for the (π^+, K^+) reaction, in contrast to the (K^-, π^-) case, where $N_{\text{eff}} = 2j_n + 1$ in PWA for the excitation of a $[(l j_n) \otimes (l j_n)^{-1}]_{J=0}$ state at $q=0$. This illustrates the role of large q in diminishing the peak cross section for (π, K) processes.

The predicted PWA cross sections to states of type (4.5) are shown in Fig. 10. Since the variation of the elementary cross section (Fig. 2) is considerably more rapid than that of N_{eff} (Fig. 9),

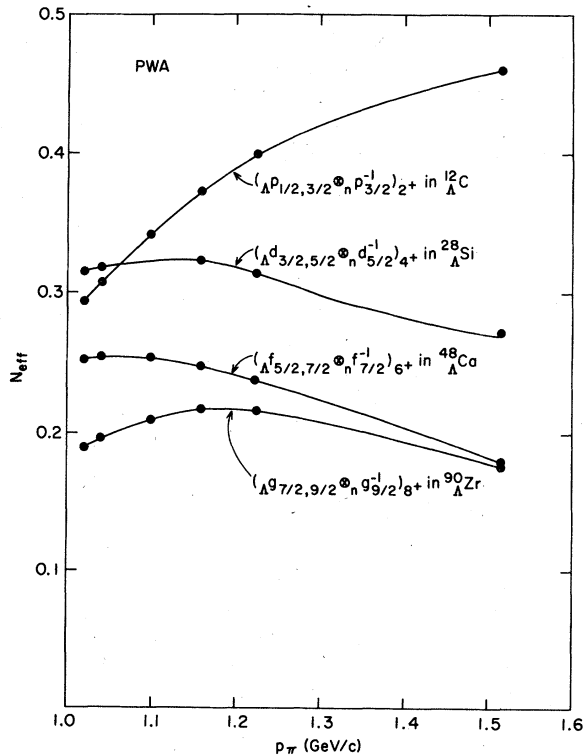


FIG. 9. Effective neutron number N_{eff} in PWA for the excitation of the high spin states of Eq. (4.5) via the (π^+, K^+) reaction, as a function of pion lab momentum p_π .

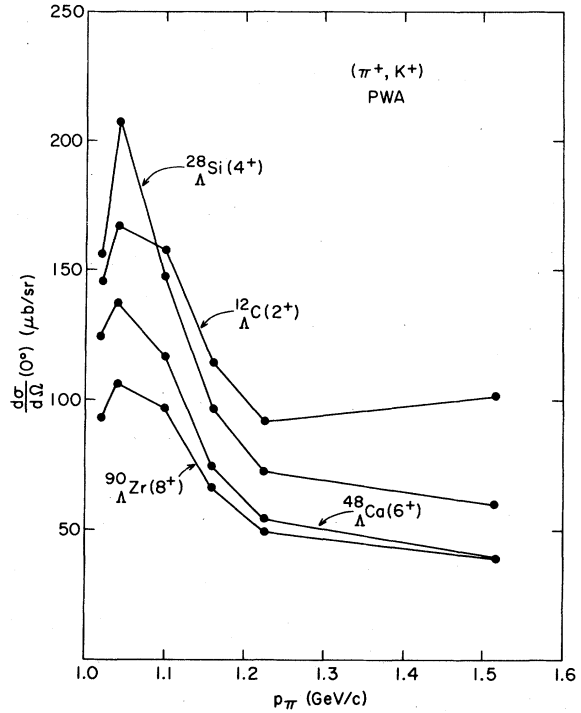


FIG. 10. Differential cross sections at $\theta_L = 0^\circ$ in PWA for the excitation of high spin states in ^{12}C , ^{28}Si , ^{48}Ca , and ^{90}Zr via the (π^+, K^+) process, as a function of p_π . The states of the residual hypernucleus are given by Eq. (4.5). We have summed over $j_\Lambda = l_\Lambda \pm \frac{1}{2}$.

the peak cross sections are obtained for values of p_π close to or slightly higher than the maximum of $(d\sigma/d\Omega_L)_{0^\circ}^{\pi^+ n^+ K^+ \Lambda}$, i.e., $p_\pi \approx 1.04\text{--}1.1$ GeV/c. We see that cross sections as large as $200 \mu\text{b/sr}$ are expected in PWA for the states of maximum J . When absorptive effects are included, these values are decreased by typically an order of magnitude or less. The peak cross sections drop somewhat as we try to form heavier hypernuclei, reflecting the increased degree of mismatch in Fig. 7.

The largest cross sections for (π^+, K^+) lead to the states shown in Fig. 10. However, the states (4.6) of one unit less in J should also be strongly populated. For these, we also have a PWA result of the form $(l_\Lambda = l_n - 1)$

$$\sum_{j_\Lambda = l_\Lambda \pm 1/2} N_{\text{eff}}^{J=2l, n-1} = \gamma_J Z^J e^{-Z}, \quad (4.8)$$

with $\gamma_J = 4/3, 6/25, 16/1323, 0.0002878$ for $1^-, 3^-, 5^-, 7^-$ states, respectively. The (π^+, K^+) cross sections to those states are shown as boxes in Fig. 11. The peak cross sections are seen to be reduced by only a factor of 1.2–1.5 relative to the maximum J states of Fig. 10, since both are stretch configurations. The observed peak heights may in fact be quite comparable, since the excitations (4.6) are probably somewhat narrower than

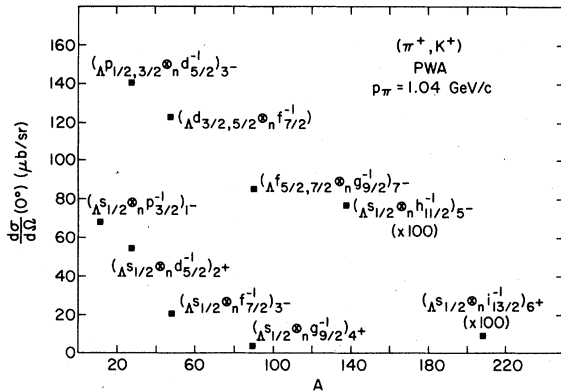


FIG. 11. Lab differential cross sections in PWA at $\theta_L = 0^\circ$ for the formation of various hypernuclear states in the (π^+, K^+) reaction at $p_\pi = 1.04$ GeV/c. We show the cross sections to the high spin states of Eq. (4.6), involving a Λ in the last bound orbit, as well as those to the ground states of Eq. (4.10).

those of Eq. (4.5), due to the fact that the Λ is in a bound state in the former ($\Gamma = 0$).

As we go away from the simple stretch states to lower spins, configuration mixing with other Λn^{-1} states becomes more important. Note that in Eqs. (4.7) and (4.8), we summed N_{eff} over the values $j_\Lambda = l_\Lambda \pm \frac{1}{2}$. For large l_Λ , the contribution of the state with $j_\Lambda = l_\Lambda - \frac{1}{2}$ dominates. For $j_n = l_n + \frac{1}{2}$, $l_n \geq 1$, we have

$$\frac{N_{\text{eff}}^{J=2l_n}(j_\Lambda = l_\Lambda - 1/2)}{N_{\text{eff}}^{J=2l_n}(j_\Lambda = l_\Lambda + 1/2)} = l_n, \quad (4.9)$$

$$\frac{N_{\text{eff}}^{J=2l_n-1}(j_\Lambda = l_\Lambda - 1/2)}{N_{\text{eff}}^{J=2l_n-1}(j_\Lambda = l_\Lambda + 1/2)} = (l_n + 1/2)(1 - 1/l_n).$$

If the Λ spin-orbit potential is indeed small, the $j_\Lambda = l_\Lambda \pm \frac{1}{2}$ states lie very close to each other in energy and are likely to be strongly configuration mixed. The ratio of N_{eff} values for the diagonalized states may then be very different from Eq. (4.9).

We have indicated above that the most strongly excited states in the (π^+, K^+) reaction will be the stretch configurations of Eqs. (4.5) and (4.6). It is also of interest to ask whether there will be a measurable cross section to configurations involving a Λ in the $s_{1/2}$ orbit:

$$(\Lambda s_{1/2} \otimes n l_{j=l+1/2}^{-1})_{J=1}. \quad (4.10)$$

In Eq. (4.10), the neutron holes l^{-1} are taken to be the same orbit considered in Fig. 10, i.e., $p_{3/2}^{-1}$ in ^{12}C , $d_{5/2}^{-1}$ in ^{28}Si , $f_{7/2}^{-1}$ in ^{48}Ca , and $g_{9/2}^{-1}$ in ^{90}Zr . For these cases, the states (4.10) will be the *ground states* of the hypernucleus. One finds in PWA

$$N_{\text{eff}}^{J=1} = \frac{(2l+2)}{(2l+1)!!} Z^l e^{-Z}. \quad (4.11)$$

The (π^+, K^+) cross sections to the ground states are plotted in Fig. 11. They are seen to be considerably smaller than the cross sections for the $J = 2l_n - 1$ states of Eq. (4.8), also displayed in Fig. 11. Nevertheless, ground states should still be measurable for $A < 60$ targets. We also show in Fig. 11 the cross sections to the $(\Lambda s_{1/2} \otimes n h_{11/2}^{-1})_5$ and $(\Lambda s_{1/2} \otimes n i_{13/2}^{-1})_{6+}$ states in ^{138}Ba and ^{208}Pb , respectively, which lie very close to the corresponding ground states [$(\Lambda s_{1/2} \otimes n 2d_{3/2}^{-1})_{2+}$ and $(\Lambda s_{1/2} \otimes n 3p_{1/2}^{-1})_{1-}$]. Even though these states are of fairly high spins, their cross sections are unmeasurably small, since we are far from the optimum J of 16 or so (in ^{208}Pb) at $p_\pi \approx 1.04$ GeV/c.

The present section provides a qualitative understanding of the physics of the (π^+, K^+) reaction, in particular the crucial role played by high spin states. In the next section, we see how distortion effects change the magnitude and angular shape of the cross sections.

V. RESULTS AND DISCUSSION

Using the formulas, approximations, and parameters given in Sec. IV, we have studied various aspects of the (π^+, K^+) reaction on light and medium weight nuclei. In this section we present and discuss the quantitative results of these studies. The section is divided into three parts. The first, A, is a set of comparative studies associated with the sensitivity of the results to the distorted waves and single particle orbitals adopted. The second part, B, presents results for different nuclear spins and/or incident pion energies. The discussion in this section concentrates on considerations associated with choosing the optimum energy and angle for studying hypernuclei via the (π^+, K^+) reaction. In the final part, C, we present and combine quasielastic Σ and Λ production results with the bound and resonance (π^+, K^+) spectrum for ^{16}O and ^{40}Ca . The results in this subsection should be representative of the experimental spectrum actually observed in the (π^+, K^+) reaction.

A. Results for different distorted waves and single particle orbitals

It is important to note at the outset that one currently has two options for calculating strangeness exchange reactions. One involves eikonal distorted waves and harmonic oscillator orbitals (usually an extremely fast and inexpensive computer code) and another option that uses fully distorted waves and either Saxon-Woods or oscillator

orbitals (a presumably more accurate but lengthy and thus expensive code in general). The former code is appropriate for calculating the complete momentum transfer, energy loss spectrum for a given nucleus while the latter code can only be used for a few isolated detailed comparisons with experiment. Thus it is important to compare results obtained using the two different approaches in order, for example, to determine the *relative* reliability of predictions relying on eikonal distorted waves and oscillator orbitals. It will turn out that such results appear sufficiently accurate that our more global predictions, presented in part C, can be made using the "eikonal-oscillator" approximations.

The first consideration is that of the effect of distortions on the magnitude and shape of differential cross sections for states of different J . The main effect of distortions would be expected to be absorption in the entrance and exit channels. In Fig. 12 we compare plane wave results (dashed lines) with fully distorted waves (solid lines) for a $(\Lambda p_{3/2} n d_{3/2}^{-1})_3^-$ state of ${}^{40}\text{Ca}$. The angular dis-

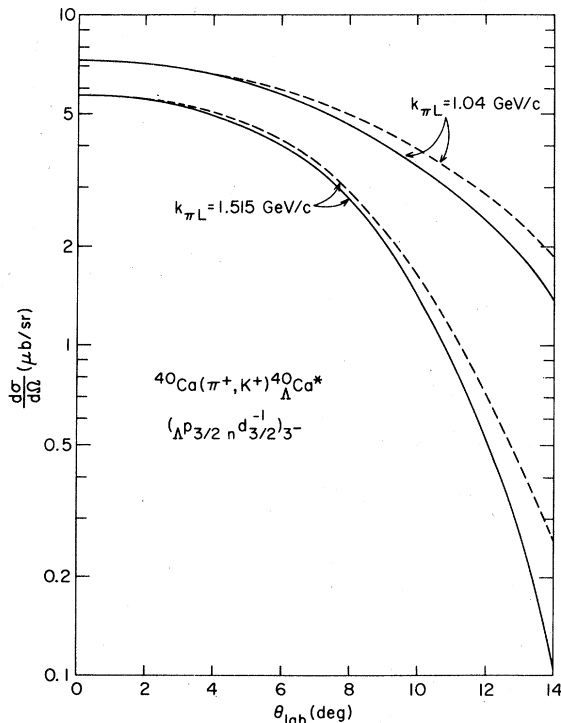


FIG. 12. Differential cross sections for the excitation of the $(\Lambda p_{3/2} n d_{3/2}^{-1})_3^-$ state in ${}^{40}\text{Ca}$ via the (π^+, K^+) reaction at $k_{\pi L} = 1.04$ and 1.515 GeV/c. The solid lines are the exact DWIA results, while the dashed lines correspond to the PWA cross sections, scaled down by constant factors 8.22 and 7.76 for $k_{\pi L} = 1.04$ and 1.515 GeV/c, respectively.

tributions are shown for two different incident pion lab momenta. The plane wave cross sections have been scaled down by the constant factors 8.22 and 7.76 for $k_{\pi L} = 1.04$ and 1.515 GeV/c, respectively. It is seen that the main effect of optical model distortions is to reduce the (π^+, K^+) cross sections by about an order of magnitude. The angular shape in the region where the cross sections are measurable (≥ 1 $\mu\text{b/sr}$) is changed in a minor way. The curves in Fig. 12 were obtained using harmonic oscillator wave functions and for the DWIA results, optical model parameters given in Sec. III. In Fig. 13 we compare several 0° plane wave cross sections with DWIA results using eikonal distorted waves (see Sec. III B) and oscillator orbitals. Depending on the state, the effect of distortions is to reduce the 0° cross section by factors of from 3 to 10. The energy dependence seen in both the PWA and DWIA results is mainly due to the energy dependence of the basic $\pi^+ + n \rightarrow K^+ + \Lambda$ process (see Fig. 2). As expected, there is a correlation between the amount of reduction resulting from absorption and the radial dependence of the original neutron orbit. The largest (smallest) reduction between the PWA and DWIA occurs for the $1s_{1/2}$ ($1f_{7/2}$) orbital which is localized closest (furthest) from the origin. There is a considerable momentum transfer to the nucleus even for forward scattering in the (π^+, K^+) reaction (see Fig. 3); as $p_{\pi L}$ increases the 0° momentum transfer gradually decreases. This effect causes the states that have the largest mismatch between the q of their cross section peak and $q(0^\circ)$ to increase slightly as a function of $P_{\pi L}$ relative to higher spin states where the q mis-

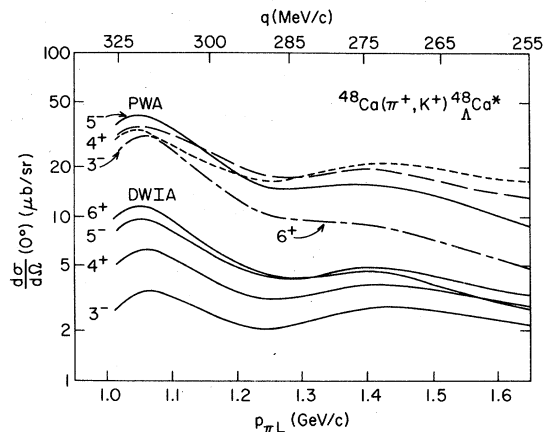


FIG. 13. Comparison of 0° cross sections for ${}^{48}\text{Ca}(\pi^+, K^+) {}^{48}\text{Ca}(J^\pi)$ as a function of $p_{\pi L}$ for $J^\pi(3^-, 4^+, 5^-, 6^+)$ in PWA and eikonal DWIA. We use oscillator wave functions with $b = 2.03$ fm. These states correspond to $\Lambda s_{1/2}$, $\Lambda p_{3/2}$, $\Lambda d_{5/2}$, and $\Lambda f_{7/2}$ coupled to $n f_{7/2}^{-1}$.

match is smaller. (Compare the energy dependence of the 3^- and 6^+ states in Fig. 13. The unusual 6^+ state decrease occurs because the zero degree momentum transfer is *below* the q required for the peak cross section for this state. Thus the q mismatch increases with increasing $p_{\tau L}$ for this particular state.)

We now consider the effect of using different orbitals on the cross section predictions. In Fig. 14 we show differential cross section calculations using harmonic oscillator (dashed lines) or Woods-Saxon (solid lines) wave functions to evaluate the radial integrals in Eq. (3.4). For a given nl_j , the orbital parameters have been adjusted to give the same rms radius. The π^+ and K^+ distorted waves are the same for the two cases. For a weakly bound Λ state such as $\Lambda d_{3/2}$, which is localized at the nuclear surface, the effect of using a Woods-Saxon wave function is to diminish the small angle cross section obtained in oscillator approximation, in this case by about 25% for the

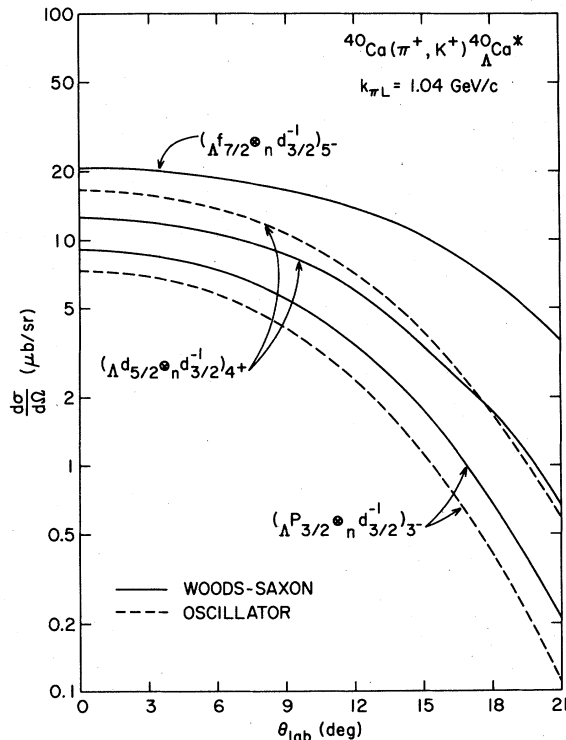


FIG. 14. Differential cross sections for the excitation of selected high spin Λn^{-1} states via the $^{40}\text{Ca}(\pi^+, K^+)^{40}\text{Ca}^*$ reaction at $k_{\tau L} = 1.04$ GeV/c. The solid curves correspond to using a Woods-Saxon potential to generate the Λ and n^{-1} wave functions, while the dashed curves are obtained using an harmonic oscillator potential. The binding energies and potential parameters are described in the text.

4^+ at 0° . A similar reduction was observed²⁰ in the reaction $^{12}\text{C}(K^-, \pi^-)^{12}\text{C}^*$ to the $(\Lambda p_{1/2, 3/2} \otimes n p_{3/2}^{-1})_2^+$ states in $^{12}\text{C}^*$, there the Λ has close to zero binding energy. The reason for the reduction is clear: the overlap $R_{i, n}(\gamma) R_{i, \Lambda}(\gamma)$ is smaller if Woods-Saxon wave functions are used, since the difference in localization radius for a strongly bound n and a weakly bound Λ is correctly given, while the oscillator potential with fixed b cannot yield this binding energy effect. Note that the situation is different for the $(\Lambda p_{3/2} \otimes n d_{3/2}^{-1})_3^-$ configuration in Fig. 14. Here both orbitals are tightly bound, and the use of Woods-Saxon wave functions actually *increases* the (π^+, K^+) cross section. The conclusion is that the use of oscillator orbitals results in an uncertainty of $\sim 25\%$ in the prediction.

The final comparison we make in this subsection is for eikonal distorted waves versus waves fully distorted in a Saxon-Woods-potential. Utilizing the parameters specified in Sec. III and Tables I and II and using oscillator orbitals in all cases, we obtain the results shown in Fig. 15. The results indicate that typical differences are about 10–20% in overall magnitude with the eikonal results having a slightly flatter angular distribution at large angles. We have also compared the eikonal predictions for $^{12}\text{C}(K^-, \pi^-)^{12}\text{C}$ with those obtained in Ref. 20 using fully distorted waves. The 10–20% difference also persists in that comparison. Thus, compared with other uncertainties in the predictions (such as the validity of the DWIA, uncertainties in the basic form for the body interaction and the appropriate nuclear structure), the inaccuracies admitted using eikonal distortions are not severe. For detailed comparison with

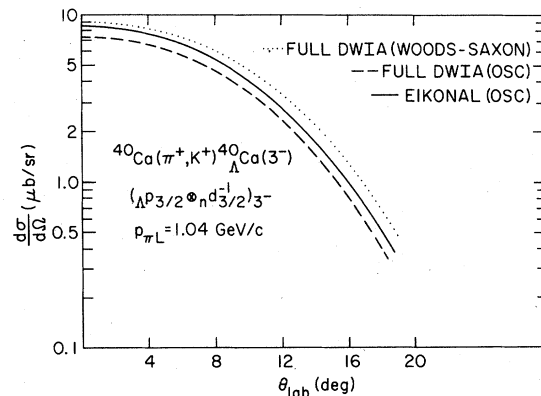


FIG. 15. Comparison of the eikonal-DWIA cross section with oscillator wave functions and the full partial wave expansion of DWIA with both oscillator and Woods-Saxon wave functions for a 3^- state in ^{40}Ca . The oscillator parameter b was taken to be 2.03 fm.

experimental results one may require the precision of fully distorted waves; However, for the global studies presented here the eikonal approximation is adequate and due to its computational convenience has been adopted.

B. Dependence of cross section on J^π and $P_{\pi L}$

As discussed in Sec. IV for plane wave results, the large forward angle momentum transfer favors high spin states. Forward angle experiments guarantee that only normal-parity high spin states will dominate the nuclear response. In Figs. 16 and 17 we show typical angular distributions for $^{16}\text{O}(\pi^+, K^+)_{\Lambda}^{16}\text{O}^*$ and $^{48}\text{Ca}(\pi^+, K^+)_{\Lambda}^{48}\text{Ca}^*$ using eikonal distortions and oscillator orbitals. As discussed earlier, the results are not qualitatively different, as far as angular distribution shapes are concerned, from plane wave results. Thus, except for the $0^+(\Lambda^1 p \otimes \pi^1 p^{-1})$ state in ^{16}O which reached a second maximum at $\sim 12^\circ$ laboratory-angle, most states studied have similar decreasing angular distributions. [The $0^+(1p, 1p^{-1})$ state cross sections are not generally expected to be

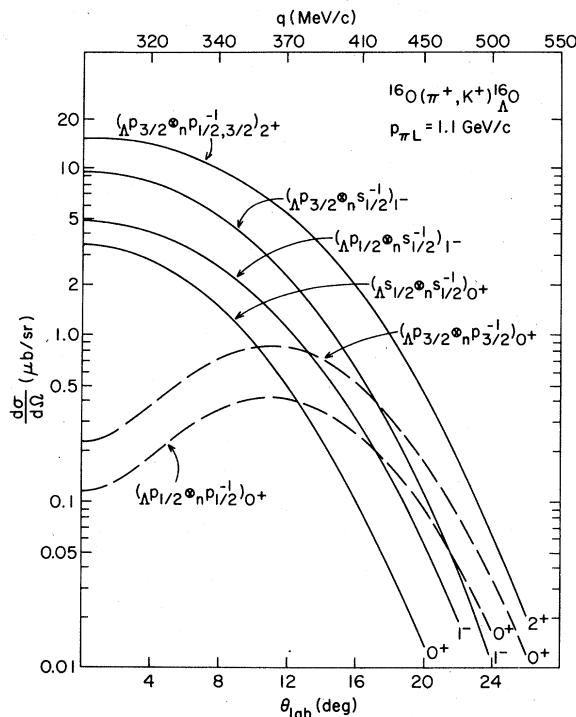


FIG. 16. Comparison of the (π^+, K^+) differential cross section for different configurations of ^{16}O at $P_{\pi L} = 1.097$ GeV/c. The oscillator parameter $b = 1.71$ fm was used in generating the eikonal-DWIA predictions. Note that the momentum transfer q is plotted on the upper-horizontal scale.

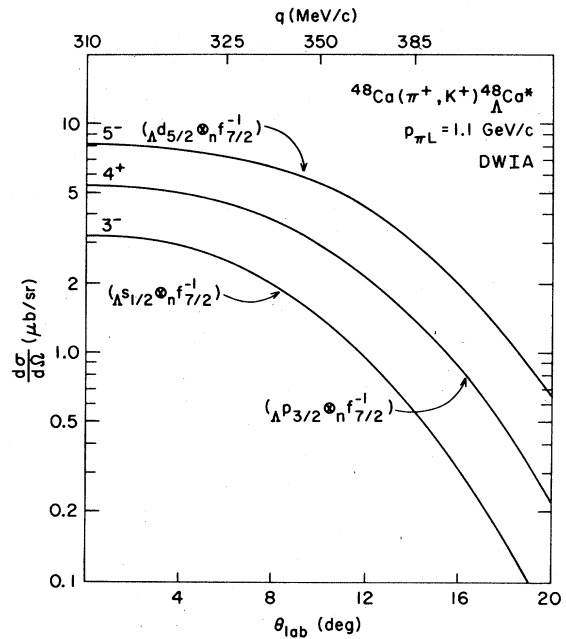


FIG. 17. Cross sections for a selected set of high spin states in ^{48}Ca , showing the relative size of the differential cross sections for single particle-hole configurations in the eikonal-DWIA.

observable at the high q associated with the (π^+, K^+) reaction.] Thus to obtain larger counting rates, one should concentrate on the region near 0° . In principle, a measurement of the angular shape can yield spin information when combined with excitation energy systematics obtained for lower spin states studied in the (K^-, π^-) reaction. In (K^-, π^-) reactions with small q , the situation is much more favorable, since $d\sigma/d\Omega$ peaks at a finite value of θ_L , and states of J differing by one unit are easily distinguishable.²⁰

In determining the optimum $p_{\pi L}$ for carrying out initial (π^+, K^+) studies there are several considerations. Two of the most important are: (a) working in a region where counting rates are highest and the cross sections do not fall too rapidly for finite angles (since often actual measurements may be made at small but finite angles $\sim 10^\circ$) and (b) choosing the kinematic region so that one has the most confidence in the input parameters and theoretical formalism adopted. In Fig. 18 we show the different angular distributions as a function of incident pion laboratory momentum, leading to the (typical) state $^{40}\text{Ca}^*(\Lambda^p_{3/2} \otimes d_{3/2}^{-1})_{3-}$. The 0° cross sections for several states in $^{48}\text{Ca}^*$ are shown in Fig. 13. Compare Figs. 1 and 2 showing the energy dependence plus transformation factors for the two body cross section. The comparison reveals that the dominant effect in deter-

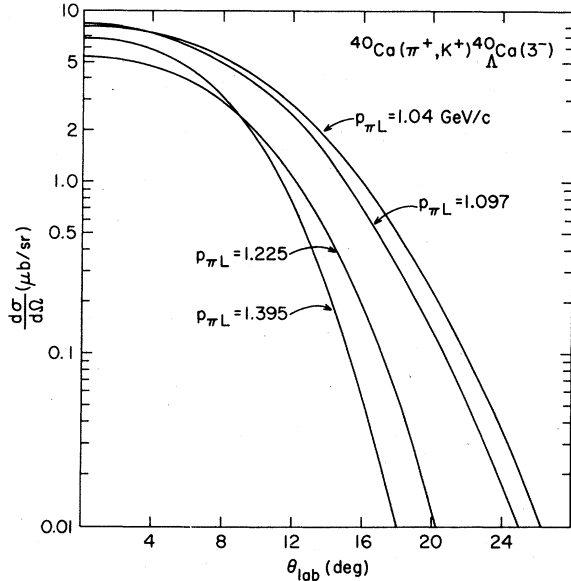


FIG. 18. Pion laboratory momentum dependence of the angular distribution for the (π^+, K^+) reaction to the $(\Lambda P_{3/2} \otimes n d_{3/2}^{-1})_3^-$ configuration of ^{40}Ca .

mining the energy dependence of the forward angle differential cross section is simply the energy dependence of the two body input. The gradual change in distortion parameters and the forward angle momentum transfer are of secondary importance. Of course at higher energies the cross sections fall off more rapidly as a function of angle (see Fig. 18). The peak cross sections occur at approximately 1.05 GeV/c. However, at this energy the elementary cross section varies rapidly with energy and Fermi averaging of the input could significantly decrease the predictions. One may prefer the momentum region ~ 1.1 – 1.2 GeV/c where the cross sections are only slightly reduced but target nucleon motion should introduce less uncertainty into the predictions.

C. Predicted spectrum for ^{16}O and ^{40}Ca

Using eikonal distortions and harmonic oscillator orbitals, we have calculated the excitation spectrum for pure Λ particle-neutron hole states reached via the (π^+, K^+) reaction. In addition the quasielastic background, discussed in Sec. III C, has been calculated using Eqs. (3.36)–(3.41).

We consider the ^{16}O case first. The oscillator parameter used was $b = 1.81$ fm. The parameter σ for the distorted waves was calculated from Eq. (3.25) and the values in Tables I and II. The neutron hole was allowed to be in the $(1p_{1/2})$ or $(1p_{3/2})$ orbitals. The single neutron hole energies were obtained from the spectrum of ^{15}O and are

given, for example, in Ref. 28. The Λ orbital was allowed to be in the $1s_{1/2}$, $1p$, $2s$, or $1d$ shell. The Λ single particle energies were obtained from the self-consistent calculations of Rayet.³⁰ Based on the experimental data from $^{16}\text{O}(K^-, \pi^-)^{16}\text{O}$ (and in reasonable agreement with the self-consistent calculations) the continuum threshold is begun at $E_{\text{ex}}^\Lambda - E_{\text{g.s.}}^\Lambda = 14$ MeV. Since the pure p-h states have not been mixed via a residual interaction in these preliminary calculations the results given are only a rough guide. The p-h contributors to each major concentration of strength are shown in Fig. 19. In each case the largest normal parity spin state dominates a given complex. States above the continuum threshold (and states whose energy is above threshold for a subsequent $\Lambda + N \rightarrow \Lambda' + N'$ interaction with an initially bound nucleon going into the

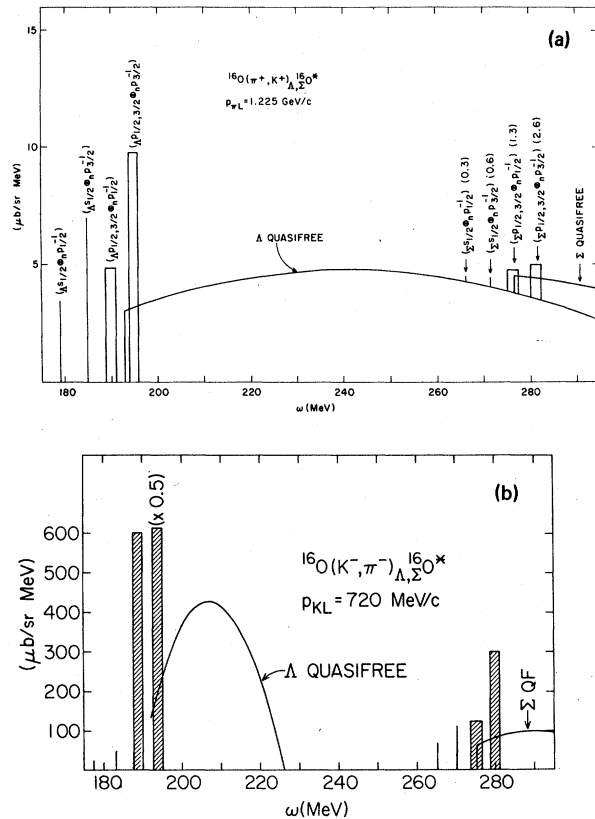


FIG. 19. (a) Predicted spectrum of the $^{16}\text{O}(\pi^+, K^+)$ process at $P_{\pi L} = 1.225$ GeV/c including Λ and Σ^0 hypernuclear excitations and the quasielastic background as a function of the energy difference $\omega \approx E_{\pi^+} - E_{K^+}$. (b) Predicted spectrum of the $^{16}\text{O}(K^-, \pi^-)$ process at $P_{K L} = 720$ MeV/c and $\theta_L = 0^\circ$, including Λ and Σ^0 hypernuclear excitations and the quasielastic background as a function of the energy difference $\omega \approx E_{K^-} - E_{\pi^-}$.

continuum and the Λ cascading down to a lower orbit) have arbitrarily been given 2 MeV widths. The value of the Fermi momentum used in the quasielastic calculations was 270 MeV/c. The elementary two body $\pi^+ + n \rightarrow \Lambda + K^+$ interaction was taken to be that which is appropriate for $P_{\pi L} = 1.225$ GeV/c and is given by $d\sigma/d\Omega \approx 338$ $\mu\text{b/sr}$ (lab). For completeness the $^{16}\text{O}(\pi^+, K^+)_{\Sigma}$ ^{16}O spectrum is also shown in Fig. 19(a) (both p-h and quasielastic contributions are presented) beginning above $\omega = 267$ MeV. The Σ single particle energies were assumed to be about 3 MeV smaller than the corresponding Λ single particle energies.³³ The strength of the $\pi^+ + n \rightarrow K^+ + \Sigma^0$ interaction is taken from Ref. 34 and is given by $d\sigma/d\Omega(0) \approx 261$ $\mu\text{b/sr}$. The momentum transfer delivered to the nucleus in the region of the Λ particle-neutron hole states is ~ 294 MeV/c, while for the Σ particle-neutron hole states the momentum transfer is ~ 384 MeV/c. The results indicate that several Λ -hypernuclear p-h state complexes dominated by high spin states should be observable and easily discernible from the Λ quasielastic background. The Σ hypernuclear states will be difficult to study using this reaction. For comparative purposes we have calculated the Λ -hypernuclear and Σ -hypernuclear spectrum resulting from the low momentum transfer (K^-, π^-) reaction at beam momentum of 720 MeV/c. The results are shown in Fig. 19(b). The same nuclear structure parameters have been used as in the previous (π^+, K^+) calculations. The strength of the elementary $K^- + n \rightarrow \pi^- + \Lambda$ ($K^- + n \rightarrow \pi^- + \Sigma$) interaction is taken from Ref. 35 (Ref. 36) and is given by 3.57 mb/sr (1.92 mb/sr). The momentum transfer near the Λ particle- n hole complexes is $q \approx 37$ MeV/c, while the Σ particle- n hole complexes have typical momentum transfers of $q \approx 116$ MeV/c (see Fig. 2). In this case the low spin states associated with a given complex dominate the spectrum because of the low momentum transfer. In addition the Λ -quasielastic peak is narrow and rapidly varying with energy. This has the effect, on the one hand, of allowing a good separation of the Λ spectrum and the Σ spectrum and on the other hand making it more difficult to study Λ -particle neutron-hole complexes in the continuum.

In Fig. 20 we have shown the results of DWIA calculations for the $^{40}\text{Ca}(\pi^+, K^+)_{\Lambda}$ ^{40}Ca particle-hole and quasielastic spectrum for $P_{\pi} \sim 1.1$ GeV/c. The neutron hole energies are taken from Ref. 37 and the Λ single-particle energies from Rayet.³⁰ Again states degenerate in energy were grouped into complexes and the combined total for a given complex is shown as a spike or block.

Due to the high momentum transfer, the high spin normal parity states associated with a given

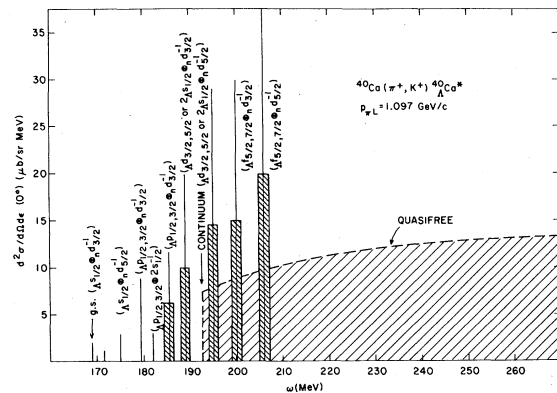


FIG. 20. Predicted excitation spectrum for $^{40}\text{Ca}(\pi^+, K^+)$ at 0° , including the quasifree background at $P_{\pi} = 1.097$ GeV/c. States in the continuum or those possessing strong interaction decay channels are given a finite width of 2 MeV to reflect their finite lifetime.

set of particle-hole orbitals dominate the associated complex. States with a path to the continuum are also arbitrarily given a width of 2 MeV. The results are quite similar to those obtained for the $^{16}\text{O}(\pi^+, K^+)_{\Lambda, \Sigma}$ processes. In addition we note that in these high q processes the quasielastic background is broad and featureless, varying only mildly with increasing ω . This should allow one to study complexes in the continuum with greater ease and less ambiguity than is possible using the (K^-, π^-) reaction. The results for the ^{40}Ca -hypernucleus spectrum are not shown, however, the conclusions are similar to the ^{16}O case, with the Σ results imposing a small perturbation on the Λ continuum spectrum.

In conclusion, we have studied the (π^+, K^+) reaction on light nuclei. Differential cross sections for strong states are on the order of tens of microbarns and thus, for example, experiments using the existing facility at Brookhaven are feasible. Because of the large momentum transfer delivered to the nucleus, high-spin, normal parity states dominate the spectrum even at very forward angles. This is in contrast to the (K^-, π^-) process, where low spin states dominate at forward angles. Another feature of the (π^+, K^+) reaction is the relative suppression and greater width of the Λ quasielastic spectrum [compared to the (K^-, π^-) Λ quasielastic spectrum]. This has the effect of making the (π^+, K^+) process more attractive than the (K^-, π^-) reaction for studying p-h complexes in the continuum. However, the greater width of the Λ quasielastic spectrum may preclude the study of light Σ -hypernuclei using the (π^+, K^+) process. Because of the complementarity and apparent feasibility of (π^+, K^+) experiments on light nuclei, we recommend that such experi-

ments be performed in the region $P_{\pi L} \approx 1.0-1.2$ MeV/c region in order to study high spin hypernuclear states.

In the future when detailed comparison with experiment is contemplated, more realistic calculations using configuration mixed Λ particle, neutron hole nuclear states should be used in the theoretical calculations. Structure calculations of this type are under study and may reveal the predicted degree of collectivity of hypernuclear states. Detailed comparison of such calculations and (K^+ , π^-)

and (π^+ , K^+) experiments offer the possibility of yielding important information regarding the Λ -nucleon interaction.

ACKNOWLEDGMENTS

We would like to thank R. H. Dalitz and H. A. Thiessen for several useful discussions. This research was supported in part (C.B.D.) by the U. S. Department of Energy under Contract No. DE-AC02-76CH00016, and partially by the National Science Foundation (L.L. and G.E.W.).

- ¹C. F. Powell, P. H. Fowler and D. H. Perkins, *The Study of Elementary Particles by the Photographic Method* (Pergamon, New York, 1959), pp. 381-400; D. H. Davis and J. Sacton, in *High Energy Physics*, edited by E. H. S. Burhop (Academic, New York, 1967), Vol. II, pp. 365-455.
- ²R. H. Dalitz, Proceedings of the International Conference, St. Cergue, 1963, CERN Report No. 64-1, 1964, pp. 158-166 (unpublished).
- ³B. Povh, *Annu. Rev. Nucl. Part. Sci.* **28**, 1 (1978).
- ⁴H. Feshbach and A. K. Kerman, *Preludes in Theoretical Physics* (North-Holland, Amsterdam, 1965), p. 260.
- ⁵R. Chrien *et al.*, *Phys. Lett.* **89B**, 31 (1979).
- ⁶Currently, kaon beams are in use at CERN, Brookhaven, and KEK in Japan.
- ⁷K. J. Nield *et al.*, *Phys. Rev. C* **13**, 1263 (1976).
- ⁸V. N. Fetisov, M. I. Kozlov, and A. E. Lebedev, *Phys. Lett.* **38B**, 129 (1972).
- ⁹E. Aslamides *et al.*, quoted by T. Bressani and A. Fainberg, in *Proceedings of the Summer Study Meeting on Kaon Physics and Facilities, Brookhaven National Laboratory, 1976*, edited by H. Palevsky, BNL Report No. 50579, p. 137; private communication from P. Gorodetsky.
- ¹⁰J. P. Vary, K. E. Lassila, and M. S. Sandel, *Phys. Rev. C*, 715 (1979).
- ¹¹Y. Cho, R. J. Holt, H. E. Jackson, T. K. Khoe, and G. S. Mavrogenes, Argonne Report No. ANL-PHY-79-2, 1979; A. M. Bernstein, T. W. Donnelly, and G. N. Epstein (private communication).
- ¹²R. D. Baker *et al.*, *Nucl. Phys.* **B126**, 365 (1977).
- ¹³R. D. Baker *et al.*, *Nucl. Phys.* **B141**, 29 (1978).
- ¹⁴D. H. Saxon *et al.*, *Nucl. Phys.* **B162**, 522 (1980); We thank Professor R. H. Dalitz for pointing out the existence of these data, and for sending us a numerical table of the cross sections.
- ¹⁵J. C. Hart *et al.*, *Nucl. Phys.* **B166**, 73 (1980).
- ¹⁶M. L. Goldberger and K. M. Watson, *Collision Theory* (Wiley, New York, 1964), p. 94.
- ¹⁷J. Hüfner, S. Y. Lee, and H. A. Weidenmüller, *Nucl. Phys.* **A234**, 429 (1974).
- ¹⁸M. K. Gupta and G. E. Walker, *Nucl. Phys.* **A256**, 444 (1976).
- ¹⁹C. B. Dover and G. E. Walker, *Phys. Rev. C* **19**, 1393 (1979).
- ²⁰C. B. Dover, A. Gal, G. E. Walker, and R. H. Dalitz, *Phys. Lett.* **98B**, 26 (1979).
- ²¹A. Bouyssy, *Nucl. Phys.* **A290**, 324 (1977).
- ²²B. R. Martin, *Nucl. Phys.* **B94**, 413 (1975).
- ²³A. A. Carter *et al.*, *Phys. Rev.* **168**, 1457 (1968).
- ²⁴P. Baillon *et al.*, *Phys. Lett.* **50B**, 387 (1974).
- ²⁵B. Povh, MPI Report No. H-1979-V25, Heidelberg, 1979.
- ²⁶H. C. Chiang and J. Hüfner, *Phys. Lett.* **84B**, 393 (1979).
- ²⁷L. D. Ludeking, Ph.D. thesis, Iowa State University, 1979 (unpublished).
- ²⁸T. DeForest, Jr., and J. D. Walecka, *Adv. Phys.* **15**, 1 (1966); R. H. Dalitz and A. Gal, *Phys. Lett.* **64B**, 154 (1976).
- ²⁹S. Calzavara and L. H. Schick, *Phys. Rev. C* **12**, 507 (1975); F. J. Bloore and E. Middleton, *Nucl. Phys.* **A190**, 565 (1972).
- ³⁰J. Rayet, *Ann. Phys. (N.Y.)* **102**, 226 (1976).
- ³¹J. Pniewski and D. Zieminska, in Proceedings of the Seminar on Kaon-Nuclear Interaction and Hypernuclei, Zvenigorod, 1977, pp. 33-50; see Table III(a).
- ³²W. Brückner *et al.*, *Phys. Lett.* **79B**, 157 (1978).
- ³³R. Bertini *et al.*, in *Meson-Nuclear Physics-1979 (Houston)*, Proceedings of the 2nd International Topical Conference on Meson-Nuclear Physics, edited by E. V. Hungerford III (A.I.P., New York, 1979), pp. 719-720.
- ³⁴R. D. Baker *et al.*, *Nucl. Phys.* **B145**, 402 (1978).
- ³⁵R. H. Dalitz and A. Gal, *Ann. Phys. (N.Y.)* **116**, 167 (1978).
- ³⁶R. Armenteros *et al.*, *Nucl. Phys.* **B8**, 223 (1968).
- ³⁷T. W. Donnelly and G. E. Walker, *Ann. Phys. (N.Y.)* **60**, 209 (1970).